Shan, B., Xiong, X., Wang, R., Zheng, Y., Yang, S. (2013): Coulomb Stress Evolution along Xianshuihe-Xiaojiang Fault System since 1713 and its interaction with Wenchuan Earthquake, May 12, 2008. - Earth and Planetary Science Letters, 377-378, 199-210

DOI: 10.1016/j.epsl.2013.06.044

# Coulomb Stress Evolution along Xianshuihe-Xiaojiang Fault System since 1713 and its interaction with Wenchuan Earthquake, May 12, 2008

Bin Shan[a] Xiong Xiong[a] Rongjiang Wang[b] Yong Zheng[a] Song Yang[a,c]

[a]State Key Laboratory of Geodesy and Earth's Dynamics, Institute of Geodesy and Geophysics, Chinese Academy of Sciences, Wuhan 430077, P. R. China

[b]GFZ German Research Centre for Geosciences, D-14473 Potsdam, Germany

[c]University of Chinese Academy of Sciences, Beijing, P. R. China

## Abstract

The curved left-lateral strike-slip Xianshuihe-Xiaojiang fault system (XXFS) in southwestern China extends at least 1400 km in the eastern margin of the Tibetan Plateau. Fieldworks confirm that the XXFS is one of the longest and most seismically active faults in China. The strain released by the slip motion on the XXFS is related to the convergence between the Indian and Eurasian plates. The entire fault system has experienced at least 35 earthquakes of M>6 in the recent 300 years and almost all segments of the system have been the locus of major historical earthquakes. Since the XXFS region is heavily populated (over 50 million people), understanding the migration of the large earthquakes in space and time is of crucial importance for the seismic hazard assessment in this region. We analyze a sequence of 25 earthquakes (M≥6.5) that occurred along the XXFS since 1713, and investigate their influence on the 2008 Mw7.9 Wenchuan earthquake occurred on the adjacent Longmenshan Fault. In our analysis, the relevant parameters for the earth crust are constrained by seismic studies. The locations and geometries of the earthquake faults as well as the rupture distributions are taken from field observations and seismological studies. Results from the Coulomb failure stress modeling indicate significant interactions among the earthquakes. After the 1713 earthquake, 19 out of 24 earthquakes occurred in the positive stress zone of the preceding earthquakes. The other 5 earthquakes located in the area without significant stress changes induced by the preceding events. In particular, we can identify 4 visible earthquake gaps with increasing seismic hazard along the XXFS, consistent with the findings from the paleo-seismological studies. The seismic activity and tectonic motion on the XXFS reduced the Coulomb stress accumulation at the hypocenter of 2008 Mw 7.9 Wenchuan earthquake, implying that the Wenchuan earthquake might not be triggered directly by the seismic activities on the XXFS. On the other hand, the Coulomb failure stress induced by the Wenchuan earthquake has increased in a region of 125-km-long segment of the XXFS, northwest of Kangding City.

**Keywords** earthquake triggering; Coulomb failure stress; Xianshuihe-Xiaojiang Fault System; seismic hazard; earthquake interaction

## 1. Introduction

The Xianshuihe–Xiaojiang Fault System (XXFS), located in southwest China, is a curved left-lateral strike–slip structure extending at least 1400 km (Allen et al., 1991) in the eastern margin area of the Tibetan Plateau (Fig. 1). Field work confirms that the XXFS, whose slip motion releases strain that is related to the convergence between the India and Eurasia plates (e.g. Molnar and Tapponnier, 1975), is one of the largest and most seismically active faults in China.

The XXFS is a complex system of active faults, including the Xianshuihe fault, the Anninghe fault, the Zemuhe fault, and the Xiaojiang fault (Allen et al., 1991; Wang and Burchfiel, 2000). The entire fault system has experienced at least 35 earthquakes of M>6 in recent 300 years and almost all segments of the system have been the locus of major earthquakes within the historic record (Fig. 1) (Allen et al., 1991). The time-space progression on XXFS evidenced by the historic earthquakes suggests certain interaction among earthquakes (Wen et al., 2008). Since the XXFS region is heavily populated (over 50 million people) (Fig. 1), understanding the spatial and temporal dependent distribution of strong earthquakes and their interaction with each other is important for assessing seismic hazard in this region.

In general, interaction between earthquakes is suggested to realize in a manner of earthquake triggering by the change of Coulomb Failure Stress (ΔCFS) (Stein, 2003): positive ΔCFS brings the fault closer to failure and thus earthquake occurrence, while negative ΔCFS retards subsequent events (Stein, 1999; Freed, 2005). Based on the earthquake stress triggering theory, numerous studies have successfully explained the features of aftershock distribution (King et al., 1994; Reasenberg and Simpson, 1992; Parsons et al., 1999; Toda et al., 1998; Wyss and Wiemer, 2000; Ma et al., 2005), time-dependent earthquakes migration (Stein et al., 1994; Hodgkinson et al., 1996; Nalbant et al., 1998), and the triggering phenomena of moderate to large earthquakes (Harris et al., 1995; Deng and Sykes, 1996; Jaume and Sykes, 1996; Martínez-Díaz et al., 2006). Based on the physical mechanisms of stress transfer, the processes of earthquake interaction are divided into static, quasi-static (time-dependent) and dynamic triggering (Freed, 2005). As mentioned above, seismic activity in stress shadow where stress accumulation is released would be depressed. Actually, stress shadow only exists in the process of static and quasi-static stress transfer. Therefore, the stress shadow effect is very important for separating static from dynamic fault interaction (Felzer and Brodsky, 2005; Felzer and Brodsky, 2006; Richards-Dinger et al., 2010). Thus, the theory of earthquake stress triggering provides us an important tool to assess time-dependent earthquake hazard (McCloskey et al., 2005; Nalbant et al., 2005).

The active seismicity and well-documented long-term earthquakes record (at scale of several hundred years) of the XXFS (Allen et al., 1991; Wen et al., 2008) make the XXFS an ideal place to analyze earthquake triggering mechanism and the earthquake migration process. Previous works (e.g., Papadimitriou et al., 2004; Paradisopoulou et al., 2007) have proven the possibility of stress interaction on the XXFS. Assuming purely elastic behavior for the crust and upper mantle and taking into account the co-seismic slip of earthquakes together with the inter-seismic loading due to tectonic stress buildup, Papadimitriou et al. (2004) and Paradisopoulou et al. (2007) analyzed the stress evolution and found that all the strong earthquakes along the Xianshuihe-Xiaojiang fault occurred on the stress–enhanced fault segments. However, both of these studies do not take into account the process of post-seismic relaxation of a viscous lower crust and upper mantle following major earthquakes, which may influence on the long term stress transfer process.

Co-seismic stress models assume purely elastic behavior for the crust and upper mantle. In reality, however, the lower crust and upper mantle behave as an inelastic body. Due to the post-seismic relaxation, the co-seismically induced stress change in the lower crust and upper mantle can be transferred upwards to the seismogenic upper crust (Lorenzo- Martín et al., 2006; Freed et al., 2007; Ali et al., 2008). Numerous studies have proposed that the stress transfer due to post-seismic relaxation may have a significant impact on the evolution of the regional stress (Deng et al., 1999; Freed and Lin, 2001; Pollitz et al., 2003; Lorenzo-Martín et al., 2006; Smith and Sandwell, 2006; Freed et al., 2007, Ali et al., 2008). Hence, post-seismic relaxation should be considered in analysis of stress transfer and earthquake interaction.

In this work, we improve the studies of Papadimitriou et al. (2004) and Paradisopoulou et al. (2007) by incorporating the stress transfer due to post-seismic relaxation. A sequence of 25 magnitude M>6.5 earthquakes (Table 1 and Fig. 1) that occurred on the XXFS over the past 300 years are used for the analysis. The purpose of this work is to study the evolution of the Coulomb stress changes along the XXFS due to co-seismic slip, post-seismic relaxation and inter-seismic tectonic loading to illuminate how the earthquake occurrence is related to these stress changes. In contrast to Papadimitriou et al. (2004) and Paradisopoulou et al. (2007), in which the sub-faults were studied independently, we study the entire XXFS as a whole fault system in this work. A more complete earthquakes catalog is employed and new knowledge from studies (Wen et al., 2008) in recent years is included to constrain the medium properties and stratification, as well as the stress build-up on the XXFS. On 12 May 2008, the Mw7.9 Wenchuan earthquake occurred on Longmenshan Fault, which is adjacent to the XXFS (Fig. 1). This earthquake and its aftershock sequence have been well studied using the seismic and geodetic data. In this study, we also calculate the stress accumulation at the hypocenter of the Wenchuan earthquake induced by the historic earthquakes on the XXFS, to investigate the impact of historic earthquakes on XXFS upon the Wenchuan earthquake, and in turn, the influence of Wenchuan earthquake upon the future seismic hazard on the XXFS.

## 2. Neotectonics and historical seismicity

*2.1 Historical earthquakes*

Although the earliest record of historical earthquakes in official documents is found as early as in the fourteenth century, the earliest seismo-tectonic investigation on the XXFS was conducted in 1934 for studying the surface rupture and damage of the 1893 and 1923 events (Wen et al., 2008). Based on the historical records, field surveys (Allen et al., 1991) and paleo-seismological studies (Wen et al., 2007), a catalogue of strong historical earthquakes on the XXFS has been available. Since early events are poorly located, evidences from the field surveys and damage reports are employed to evaluate the locations and intensities of the strong historical earthquakes. Based on well-evaluated rupture extents and intensity distributions, Wen et al. (2008) developed an empirical relationship between rupture extent and seismic intensity distribution, by which they determined the locations and spatial extents of ruptures for 36 moderate and large earthquakes on the XXFS in the last several hundred years systematically. This earthquake catalog provides an updated dataset particularly useful for studying the earthquake interactions.

In this work, we analyze the earthquake sequence compiled by Wen et al. (2008), in which 36 events are listed and classified in three categories, A, B and C, according to their reliabilities. Because of large uncertainties for the location and rupture area, 6 events classified by “C”, which may include 2 events with M>6.5, are excluded from our analysis. Another criterion for choosing event is the magnitude. The M<6.5 events are also excluded from the study because they can only perturb the stress field at local scale (tens of km) (Freed et al., 2007). Because no strong or large earthquake on secondary faults has been recorded during the last 100 years (Wen et al., 2008), our attention only focuses on the major fault zones of the XXFS rather than the secondary faults. As a result, we identify 25 historical earthquakes with M≥6.5 events (listed in Table 1 and shown in Fig.1): 14 on Xianshuihe fault, 3 on Anninghe fault and 8 on the Xiaojiang fault.

The source parameters are determined by a couple of ways: The rupture lengths, slips and focal solutions of the 1967, 1973 and 1981 events on the Xianshuihe fault are taken from seismological studies (Zhou et al., 1983a, b). For the earthquakes without good constraints on rupture lengths, widths and slips, alternate methods are applied to determine the parameters. In the case of absence of well-constrained coseismic slip distributions, the earthquake rupture faults are modeled as rectangular planar patches with uniform slip. The rupture lengths are taken from Wen et al (2008). Synchronously, we inferred width of rupture and amount of slip by estimating rupture areas with the empirical scaling laws and relationships of Wells and Coppersmith (1994). Strike, rake and dip angles are estimated based on the fault geometry from geological observations and/or focal mechanisms of recent events occurred on that fault. The source parameters associated with all 25 earthquakes in the present analysis are summarized in Table 1 and shown in Fig. 1.

*2.2 Fault kinematics*

The kinematics of the XXFS has been studied by geological investigations (e.g. Allen et al., 1991; Wang and Burchfiel, 2000; Xu et al., 2003), seismological studies (e.g. Molnar and Deng, 1984; Holt et al., 1991) and geodetic measurements (Zhang et al., 2004; Shen et al., 2005). Geological observations of the geomorphic offset of Quaternary landform exhibit a distribution of left-lateral slip rate on the Xianshuihe fault that decreases from ~15±5 mm/yr on the northwestern segment to ~9.6±1.7 mm/yr on the southeastern one (Allen et al., 1991; Xu et al., 2003). Recent GPS data suggest a contemporary slip rate of about 10 mm/yr along the entire Xianshuihe fault (Shen et al., 2005; Chen et al., 2000; King et al., 1997), which is roughly consistent with the field geological observations, and the slip-rate estimated from the moment tensors of large earthquakes in the last ~100 years (Molnar and Deng, 1984; Holt et al., 1991). On the Anninghe fault and the Zemuhe fault, the estimated Quaternary sinistral slip rates are ~6.5± 1 mm/yr and ~6.4±0.6 mm/yr, respectively (Allen et al., 1991; Xu et al., 2003), which are consistent with the GPS observations (~7 mm/yr) (Shen et al., 2005). Geological studies (Song et al., 1998; Xu et al., 2003) indicated that the average slip rate of the Xiaojiang fault decreases from ~10mm/yr on the northern and middle segments to ~3.5mm/yr on the southernmost segment, suggesting a similar slip-rate estimated by GPS measurements (Shen et al., 2005). The consistency between the slip-rates determined by geodetic and geological studies suggests that the contemporary inter-seismic strain is comparable to its long-term motion on the XXFS. The slip-rate used for inter-seismic loading calculation in this study is shown in Fig.1.

## 3. Model and methods

We conducted our study on the basis of the change of Coulomb Failure Stress (ΔCFS) (Scholz, 1990) using the expression

$$\Delta CFS = \Delta \tau + \mu' \Delta \sigma_N \qquad (1)$$

where $\tau$ is the shear stress, $\sigma_N$ is the normal stress and $\mu'$ is the apparent coefficient of friction. The change in shear stress $\Delta\tau$ is positive in direction of the slip of the following earthquake (the receiver fault); $\Delta\sigma_N$ is positive for increasing unclamping normal stress. The equation implies that regional faults that lie in areas of positive ΔCFS are brought closer to failure, whereas faults that lie in areas of negative ΔCFS are brought further away from failure (Freed, 2005). In this study, the focal mechanism of the following earthquake (as shown in Table 1), which represents the main kinetic characteristic of rupture fault, is selected to be the parameters of receiver fault in our calculation.

In this study, we build the evolution image of ΔCFS in the XXFS region by considering the contributions from co-seismic, post-seismic and tectonic loading since the 1713 earthquake occurred on the Xiaojiang fault. To calculate the co- and post-seismic stress, we used the model of dislocation sources embedded in a mixed elastic/inelastic layered half-space (Wang et al., 2003, 2006). We also employed program PSGRN/PSCMP (Wang et al., 2006), by which surface and subsurface deformation due to the common geophysical sources in a multi-layered viscoelastic-gravitational half-space can be determined.

The parameters of the layered lithospheric model used in this work are summarized in Fig. 2. The thickness of crustal layers, the density and Vp distributions are taken from seismic studies, including tomography models (Li et al., 2009; Zhang and Wang, 2009) and deep seismic sounding experiments (Li and Mooney, 1998). The quantities of density ρ and $V_P$ are used to derive the shear modulus *G* by the following expression (Aki and Richards, 2002)

$$G = \rho V_s^2 \approx \frac{1}{3}\rho V_P^2 \quad (2)$$

We assume that viscoelastic processes can only occur below 19 km depth, which is the maximum depth of earthquakes occurring in the studied area. Above this depth co-seismic stresses are assumed to be maintained, while below this depth, co-seismic stress changes within the ductile lower crust and upper mantle cannot be sustained and lead to viscoelastic flow, which tends to transfer stress upward to the seismogenic crust (Ali et al., 2008). The magnitude and pattern of post-seismic deformation and stress changes mainly depend on the rheological layering of the crust and upper mantle, which in turn depends on composition, temperature and other environmental parameters. In this study we use the linear Maxwell rheology to simulate the viscoelastic effect at decade-to-century time scales. In all the post-seismic relaxation calculations, the viscosity used is $1 \times 10^{20}$ Pa·s for the mantle and $1 \times 10^{19}$ Pa·s for the lower crust, the same rheology inferred by Shi et al. (2008) for the XXFS region. Otherwise, Wen et al. (2012) place an effective viscosity of $2 \times 10^{19}$ Pa·s on the lower crust to mantle of north Tibet based on the postseismic studies of 2001 Kokoxili earthquake. Although the constant effective viscosity is an approximation and will tend to underestimate the post-seismic strain rate and the stress changes in the early post-seismic period, it does not change the fully relaxed state (Freed et al., 2007). Therefore, considering that most post-seismic relaxation processes associated with historic earthquakes are either completed or nearly completed at present, the use of the linear viscosity should not strongly affect the estimate of stress changes induced by the post-seismic relaxation. To verify our assumption, we also tested other viscosity values.

We model the tectonic stress loading following a procedure outlined by Lorenzo-Martín et al. (2006). The tectonic stress loading was realized by a steady slip over the depth range 19 to 100 km, and the deep dislocation technique proposed by Savage (1983). The slip increases from zero at 19 km depth to its full magnitude at a depth of 43 km. The magnitude of the slip on the XXFS is indicated by color solid line overlapping on segments of the fault (Fig. 1). However, the model given by Savage (1983) assumes semi-infinite slip, requiring extending the dislocations to > 1000 km to avoid decay of velocities back to zero at lager distances. Therefore, the rate of inter-seismic tectonic loading would be underestimated based on the 100 km extent of deep-slip dislocation. Moreover, the sharp termination at 100 km depth may be inconsistent with the large-scale interseismic GPS velocities, and the linear tapering of the deep-slip in the lower crust and upper mantle is a simple approximation which may produce certain additional uncertainty, but we think that the fine distribution of the deep-slip at depth as large as 100 km should not modify substantially the stress loading in the upper crust.

The apparent coefficient of friction $\mu'$ is set to be a moderate value, 0.4 (King et al., 1994). Different values of $\mu'$ were tested to verify the stability of results. In contrast to the commonly used ΔCFS representations in map view, we follow the concept of Nalbant et al. (1998) calculating and displaying ΔCFS accumulation only at the rupture planes and faults. These cumulative ΔCFS values are calculated at a depth of 10 km in 2-km spacing, taking into account the varying orientation of XXFS and rupture planes of historical earthquakes.

## 4. Numerical results

*4.1 Stress transfer and accumulation on the XXFS*

*4.1.1 Stress transfer and earthquake interaction on the XXFS*

We calculate the Coulomb stress change on the rupture faults of the events posterior to 1713 and assess the influences of co- and post-seismic ΔCFS. To assess the interactions and triggering effects among the historical earthquakes occurred on the XXFS, the influence of tectonic loading is ignored in this section. We regard positive stress values below 0.01 MPa as not significant, since steady tectonic loading can cause such amounts of stress over a very short period of time (Stein et al., 1997). Table 2 compiles values for the maximum and average stress change at the rupture plane, and the percentage P of the rupture length with ΔCFS≥ 0.01MPa is also displayed in this table. The values in Table 2 display the state immediately before the corresponding event. In order to examine the contributions from co- and post-seismic components in details, the co- and combined (co- and post-seismic) change of CFS are summarized in Table 2, too.

We regard positive stress values lager than 0.01 MPa, which is the proposed threshold value suggested for earthquake triggering (King et al., 1994; Stein 1999; Heidbach and Ben-Avraham, 2007), as a significant encouragement of subsequent earthquakes by preceding events. The results are classified according to the following scheme: If the rupture fault of the succeeding earthquake experienced a mean/maximum ΔCFS≥0.01 MPa, the earthquake is classified as a probably encouraged event by the stress changes of the preceding earthquakes. Based on this criterion, if only the process of static stress transfer is taken into consideration, 15 out of 24 earthquakes posterior to 1713 in Table 1 show potential encouragement due to the maximum ΔCFS values, and only 4 out of 24 earthquakes due to mean ΔCFS values. If we further consider the joint effect of elastic and viscoelastic loading on the rupture faults, 19 out of 24 earthquakes exhibit significant encouragement due to the maximum ΔCFS values, and 7 out of 24 earthquakes could be significant encouraged by the mean ΔCFS values (Table 2). The central coordinates of the rupture surfaces determined by the maps of distributions of seismic intensities and relative severely damaged areas (Wen et al., 2008) are listed in Table 1. Usually, whether the succeeding events would be triggered is determined by the maximum ΔCFS on the receiver faults. Therefore, the maximum ΔCFS on the rupture fault could be taken to judge whether the earthquake is a potential encouraged event or not. Although the maximum co-seismic ΔCFS on the rupture surface of 1725a (8/1/1725) earthquake is only 0.009 MPa, the post-seismic relaxation plays a more important role on increasing the CFS accumulation. Since the ΔCFS caused by post-seismic relaxation increases with time, which will be expected to be dominative for raising the probability of earthquake occurrence of the 1725a earthquake, as well as the 1763, 1955 and 1981 earthquakes.

In our model the remaining 5 earthquakes located in regions where the maximum combined ΔCFS (co- and post-seismic stress changes) is lower than 0.01 MPa. Although the maximum CFS increment on the ruptures of these five earthquakes caused by preceding earthquakes is positive, the magnitudes of maximum/mean stress changes are rather small ($10^{-3}$~$10^{-4}$ MPa). In the historical earthquake catalog, the 1725b earthquake (1725-8-1) is the first event occurred on the Xianshuihe fault, and the 1732 event is the first event occurred on the Anninghe fault. The 1733 event located at the north end of the Xiaojiang fault, and its preceding events (1713, 1725a) occurred on the middle segment of the Xiaojiang fault. The 1747 and the 1811 earthquakes on the Xianshuihe fault are about 200 km away from the 1725b event. The 1811 earthquake occurred at the northwest end of the Xianshuihe fault (Fig. 1). Therefore, the low magnitudes of maximum CFS increment on the rupture plane of these five earthquakes are due to the long distances between the rupture planes and the preceding events. Notice that the 5 events discussed above are the earlier events of the catalog used. It is unknown how these earthquakes are related to the earthquakes before 1713.

Considering the effect of co- and post-seismically induced stress changes, stress evolution processes along the rupture surfaces of six typical earthquakes are calculated. The spatial step of the ΔCFS distribution is 1 km and the variations of focal mechanisms are also taken into account. Figure 3 shows the results for the earthquakes of 1763, 1789, 1833, 1850, 1893 and 1952, respectively. Dash line represents the ΔCFS immediately before the earthquake, and the solid line represent the ΔCFS immediately after the earthquake. The distance between dash line and solid line in same color represents the co-seismic impact of the event in this year, and the distance between two adjacent lines in different color represents the post-seismic relaxation during the time between the two events. To make the figures more concise, only the preceding events with effectively stress influences are taken into account. It is shown that the maximum ΔCFS on the rupture fault of the 1763 earthquake is below 0.002 MPa immediately after the 1733 earthquake, but it is raised to more than 0.02 MPa before the occurrence of the 1763 earthquake because of post-seismic relaxation, which is about twice of the threshold for earthquake triggering. Table 2 also shows that while taking into account the post-seismic effect, the maximum/mean ΔCFS on the rupture plane of 1763 earthquake are both higher than 0.01 MPa. Therefore, the post-seismic relaxation is mainly responsible for increasing the ΔCFS in the encouragement of 1763 earthquake.

Ignoring the abnormal jump due to edge effects and rupture configuration, although the middle part of the segments of the 1789, 1833 and 1850 earthquake located on the stress shadow, the two ends of their rupture planes have the positive ΔCFS values much higher than the threshold of earthquake triggering. Therefore, the maximum stress changes of several earthquakes in Table 2 are higher than 0.01 MPa, but the mean values are lower than 0.01 MPa. Several previous studies have proven that CFS increment only on one end of rupture plane of receiver fault can also trigger succeeding earthquakes (Nalbant et al., 2005). It is shown that the stress accumulation on the rupture of 1893 earthquake is initiated by the co-seismic slip of the 1725 earthquake on the Xianshuihe fault zone, with the maximum CFS increment of 0.1 MPa on the south end of the rupture surface. Then the post-seismic relaxation gradually enhances the ΔCFS accumulation on the entire rupture plane, until the accumulated stress on the southern part is partly released by 1748 earthquake. In addition, the 1792 event further raises the stress accumulation on the north part of the rupture plane. The ΔCFS on the rupture surface of 1893 earthquake is substantially enhanced subsequently. As a result, the ΔCFS is raised about 0.45 MPa at the north end of the rupture fault and 0.3 MPa at the south end immediately before the 1893 earthquake occurrence. The 1952 earthquake is mainly impacted by the 1786 and 1850 earthquakes, which enhance the stress accumulation on northern and southern segments of the rupture plane of the 1952 event, respectively. Similar to the 1893 earthquake, the post-seismic relaxation also plays a more important role for increasing the CFS accumulation. With time passes by, the post-seismic relaxation is expected to be dominative for raising the seismic hazard on this segment.

*4.1.2 Stress accumulation and seismic hazard on the XXFS*

We extend our calculation to the year of 2008 to study how the ΔCFS accumulates on the XXFS recently. Figure 4 shows the present-day stress state for each fault segment with a comparison between the results with and without the contribution from the tectonic loading. A remarkable feature of the accumulated ΔCFS is the existence of four zones, A-D, with significant CFS increment. Notice that we do not include the northernmost segment of XXFS that also exhibits CFS increment because the stress accumulation and seismic hazard on this segment would also be strongly influenced by the earthquake activity on the Ganzi-Yushu fault system. The segments A-D are consistent with the four seismic gaps in the study of historical earthquake (Wen et al., 2008), which were obtained by analyzing the average recurrence intervals and time elapsed since the latest events on the individual fault segments.

The segment A is located at the XXFS between Daofu County and Kangding City. In comparison, Wen et al. (2008) separated the segment A into 4 individual fault segments S3-S6, but only recognized the segment S5 as the first seismic gap in the middle Xianshuihe fault zone. In Fig. 5a, the co-seismic ΔCFS (green line) is negative on two ends of this segment. The only region with significant positive co-seismic ΔCFS appears in the middle of the segment. When both the post-seismic relaxation and the tectonic loading process are taken into account, the sum of the earthquake-induced ΔCFS (red line in Fig. 5a) on the majority part of the Kangding-Daofu segment is about 0.8 MPa, and the integrated stress change (co-, post-seismic stress change and tectonic loading) is larger than 1.2 MPa. Therefore, we assess the seismic hazard at the entire segment A to be considerably higher than that given by the historical earthquake study (Wen et al., 2008).

The segment B is located between Shimian County and Xichang City, and extends along the second seismic gap, segments S8 and S9, of the Anninghe fault zone (Wen et al., 2008). After removing the edge effects (Fig. 5b), the northern and southern sections of the segment B are under positive earthquake-induced cumulative ΔCFS with magnitudes of ~0.4 and 0.6 MPa, respectively, while the middle part is still negatively stressed. However, when the tectonic loading process is taken into account, the stress shadow on the segment B disappears and the ΔCFS on the entire segment B is increased with magnitudes most exceeding 1 MPa. Although a magnitude 6.7-6.8

earthquake occurred on segment S9 in 1952, its rupture fault is too small to release the strain accumulated in the second gap (Fig. 4b). According to (Wen et al., 2008), the last two strong earthquakes on the segment B occurred probably in 1480 and 1536. Therefore, we assume that significant tectonic stress have been accumulated in the segment B, resulting in a high seismic hazard there.

The segment C is located between Dongchuan City and Songming County and is distributed along the segment S12 of Xiaojiang fault zone (Wen et al., 2008). In Wen et al. (2008), the segment S11, north to the segment S12, was recognized to be the third earthquake gap. Although the last major earthquake occurred on the segment S11 in 1733, the majority of this segment is still located in the stress shadow. The last major earthquake on the segment S12 occurred in 1833, with magnitude larger than the one in 1733. Based on our calculations, the co-seismic $\Delta$CFS since 1713 is negative on the whole area of segment C (green line in Fig. 5c). However, the time-dependent stress accumulation due to the viscoelastic relaxation and tectonic loading processes has reached $\Delta$CFS $> 0.5$ MPa on the south part of the segment C.

The segment D is the southernmost segment of the Xiaojiang fault zone where no major earthquake has occurred since 1606 (Wen et al., 2008). The final stress state in 2008 (Fig. 4) indicates that the segment D has accumulated earthquake-induced and combined (co-, post-seismic stress change and tectonic loading) $\Delta$CFS of ~0.2 and ~0.5 MPa over a length of ~90 km. Following empirical equation (Wells and Coppersmith, 1994) this segment is capable of generating a Mw7.4 earthquake.

### *4.2 Stability of the results*

In this sub-section, we estimate the influences caused by the uncertainty of parameters in the numerical models. Using different effective coefficients of friction and viscosities of lower crust and upper mantle, we calculate the percentage of the rupture length with ΔCFS≥ 0.01MPa of the earthquakes which occurred after 1713. The values are given in Table 3 showing the state immediately before the occurrence of the corresponding event.

*4.2.1 Effect of effective coefficient of friction*

The choice of an appropriate value for the effective coefficient of friction μ' is of importance for the model, because it modulates the contribution of the normal stress to the CFS calculation. Usually, the coefficient μ' varies with the types of faults: high values (0.6-0.8) for thrust and normal faults, while lower values (0.2-0.4) for strike slip faults (Xiong et al., 2010). Whereas, Parsons et al. (1999) found low value of effective friction for high-angle, strike-slip faults, and high value for oblique faults. In the previous sections, the moderate value of 0.4 is chosen for the numerical calculations.

In the left part of Table 3, our numerical tests show that some changes can be observed in the calculated stress field with different values of μ'. For most of the historical earthquakes, the percentage of their fault part with ΔCFS≥ 0.01MPa varies usually less than 5% when changing μ' between 0.2 and 0.6. However, there exist some extreme cases, in which quite large changes can be observed and needed to be notified. When the co- and post-seismic stress of the preceding earthquakes on the 1811 rupture surface is taken into consideration, the percentage increases from 0.0% for μ' =0.2 to 31.2% for μ' =0.6, implying that for larger value of μ', the 1811 earthquake might be recognized as significant encouragement by preceding earthquakes. The co- and post-seismic stress of the preceding earthquakes on the 1909 rupture fault also increases the percentage from 19.5% for $\mu'$ =0.2 to 31.7% for $\mu'$ =0.6. Among all the events, the changes caused by the variation of $\mu'$ is largest for 1967 earthquake because of its mid-angle dip and oblique slip direction, in which the percentage increases from 15.8% for $\mu'$ =0.2 to 57.8% for $\mu'$ =0.6. Since the XXFS is a strike-slip fault with significant cumulative strike slip, shear stress changes dominate over normal stress changes, the $\Delta$CFS accumulation is basically governed by shear stress component. Therefore, we choose the moderate value of $\mu'$ (0.4) for stress modeling. Moreover, the focal mechanisms in Table 1 reveal that the 1811 and 1967 earthquakes are left-lateral strike-slip events with plenty of thrust component; a larger value of $\mu'$ (e.g., 0.6) may be more reasonable for these two earthquakes.

*4.2.2 Effect of Viscosity*

Since viscoelastic relaxation is introduced, the viscosities of the lower crust and upper mantle are of importance for calculating the time-dependent stress field. In this study, we choose the viscosities according to the results from studies on post-seismic deformation (Shi et al., 2008). Due to lack of continuous observation of post-seismic deformation in the studied area, the viscosities of the crust and upper mantle are not well constrained. Therefore, we try different choices of viscosities to test the stability of the results. The right side of Table 3 shows the results of the test experiments with various configurations of viscosities.

We first fix the viscosity of upper mantle ($\rho_m$) at $10^{20}$ Pa·s and test how the percentages of co- and post-seismic $\Delta$CFS$\geq$ 0.01MPa on the rupture fault of most earthquakes (Table. 3) varies with the viscosity of lower crust ($\rho_c$). Numerical results show that only slight decreases of the percentage can be observed in a fraction of events with increased $\rho_c$. In turn, if fixing $\rho_c$ but varying $\rho_m$, the changes in the percentage are negligible.

In the lower crust and upper mantle, the high pressure and temperature prevent rock from failing in a brittle manner. Following the co-seismic elastic deformation, viscous flow is induced by the co-seismic stress change (Kirby and Kroenberg, 1987; Freed, 2005). Due to the visco-elastic relaxation, the stored elastic strain is transferred upward to the seismogenic upper crust, leading to increased stresses in a wider distance range (Freed, 2005). The speed of the stress transfer is controlled mainly by the viscosity of the lower crust: the smaller the viscosity, the quicker the transfer speed. When fixing $\rho_m$ at $10^{20}$ Pa·s, our numerical results are almost same for $\rho_c$ smaller than $10^{18}$ Pa·s that corresponds a characteristic relaxation time less than a few years, implying that the stored elastic strain in lower crust and upper mantle might be completely relaxed during the inter-seismic transfer process if $\rho_c$ ~$10^{18}$ Pa·s or less. On the other hand, a viscosity value considerably higher than $10^{19}$ Pa·s for the lower crust is not supported by geodetic observations of the post-seismic deformation. Therefore, we conclude that the uncertainties of viscosities of lower crust and upper mantle do not significantly influence on the numerical results presented in the present paper.

### *4.3 Influence of the historical seismicity of XXFS on the Mw7.9Wenchuan earthquake*

On May 12, 2008, the great Wenchuan earthquake (Mw7.9) ruptured about 300km of the Longmenshan fault, one of the most active seismic zones in Southwest China. The earthquake destroyed millions of buildings and killed tens of thousands people. The epicenter of the Wenchuan earthquake is located at (31.0°N, 103.4°E) by the China Earthquake Networks Center

(CENC). The Longmenshan fault zone is a complex system of faults that collectively accommodate the crustal deformation in eastern Tibet induced by the Indo-Asian collision. In the past several centuries, numerous major earthquakes occurred in the Longmenshan fault system and the neighboring faults (Luo and liu, 2010).

Since the Xianshuihe fault zone is only about 150 km from the epicenter of the Wenchuan earthquake, it has been debated whether the 2008 Mw7.9 earthquake was triggered by the historical earthquakes occurred on the XXFS, and vice versa, whether the seismic hazard on the XXFS is increased after the Wenchuan earthquake. Using the slip models inverted separately or jointly from seismic and geodetic data and field observations as well (Ji and Hayes, 2008; Wang et al., 2008), Parsons et al. (2008), Toda et al. (2008) and Shan et al. (2009) estimated the co-seismic Coulomb stress changes and evaluate the seismic hazard on the surrounding major faults in the region soon after the Wenchuan earthquake. All of their studies show that earthquake hazard on the Xianshuihe fault zone is raised by the static stress changes caused by the Wenchuan earthquake. In the following sub-sections, we first estimate the influence of the historical earthquakes of the XXFS on the Wenchuan earthquake. Then we model the ΔCFS accumulation on the XXFS caused by the Wenchuan earthquake and compare it with the cumulated stress induced by the historical seismicity and tectonic loading obtained in the previous section. The time-dependent viscoelastic relaxation of lower crust and upper mantle on the XXFS caused by the Wenchuan earthquake will be discussed, too.

#### *4.3.1 Influence from the historical seismicity of XXFS on the Mw7.9Wenchuan earthquake*

Figure 6 shows the temporal evolution of the accumulated stress at the hypocenter of the

Mw7.9 Wenchuan Earthquake prior to its occurrence. In our model, the parameters of receiver fault are determined by the focal mechanism of Wenchuan earthquake (Wang et al., 2008). The strike, dip and rake angles are 229°, 32°, and 118°, respectively. The green and the red lines represent the normal and shear stress change. The corresponding $\Delta$CFS accumulation at the hypocenter for the effective coefficients of friction $\mu' = 0.6$ and 0.8 are displayed by blue and black lines, respectively. Because the Wenchuan earthquake is a thrust event with small right-lateral strike slip component, high values of friction coefficients (0.6 and 0.8) for thrust and normal faults (Xiong et al., 2010) are selected in the comparison. The focal depth of Wenchuan earthquake is still debated. While CENC advocated an estimate of 14.5 km for the focal depth, (Zhang, 2010), Liu et al. (2009) proposed a value of 19 km by relocating with the observations of the Western Sichuan Seismic Array (WSSA). In the study, we calculate the stress evolution for both depths of 14.5 km and 19 km, and show the correspondent results by the solid and dash lines in Fig. 6.

Figure 6 shows that the cumulated stress at the hypocenter of the Wenchuan earthquake is mainly influenced by the historical earthquakes on the Xianshuihe fault zone, especially the 1786, 1816, 1955 and 1973 earthquakes. Although the $\Delta$CFS on the hypocenter of 14.5 km depth keeps positive for 44 years prior to 1830, after 1830 the cumulated $\Delta$CFS on the hypocenter at the depth of 14.5 km and 19 km for both $\mu'$ ~0.6 and ~0.8 are always released by the previous earthquakes on the XXFS. Before the occurrence of the Wenchuan earthquake, the $\Delta$CFS at the hypocenter varies from 0.013 to 0.02 MPa depending on different parameters choices. The normal stress changes at the hypocenter are positive, and would encourage the fault to rupture. In the contrary, the negative shear stress changes $\Delta\tau$ inhibit the occurrence of the Wenchuan earthquake. Although the higher value of effective coefficient of friction would enhance the contribution of the normal stress to the ΔCFS, the ΔCFS are always negative at the hypocenter of the Wenchuan earthquake, even if the maximum theoretic value of μ' ~1.0 is used. Therefore, the influence of the historical earthquakes of the XXFS on the Wenchuan Earthquake is negligible.

*4.3.2 Influence of the Mw7.9Wenchuan earthquake on seismic hazard of XXFS*

Usually a large earthquake can perturb regional stress field and may enhance the seismic hazard in neighboring regions and faults (e.g., King et al., 1994; Lin and Stein, 2004; Stein, 1999). After the Wenchuan earthquake, several studies (Parsons et al., 2008; Toda et al., 2008; Shan et al., 2009) have calculated the static ΔCFS accumulation on major faults around the Longmenshan region. Parsons et al. (2008) shows that the ΔCFS accumulation on Xianshuihe fault increases more than 0.01 MPa over a 125-km length from the junction between the XXFS and the Longmenshan fault system. Toda et al. (2008) suggest a 0.02-0.05 MPa increase within the 1893 and 1955 rupture zones of the Xianshuihe fault between Daofu and Kangding, which is also recognized by Shan et al. (2009). In this study, we calculate the ΔCFS on the Xianshuihe fault zone using the slip models given by Ji and Hayes (2008) and Wang et al. (2008), respectively, and compare the numerical results with the cumulated stress induced by the historical seismicity on XXFS and tectonic loading estimated in the previous section.

As shown in Fig. 7, the Wenchuan earthquake enhances the Coulomb stress accumulation over a segment of about 125 km length, from the junction of the Xianshuihe fault and the Longmenshan fault system to the northwest of the XXFS between Daofu County and Kangding City. The maximum increased ΔCFS on the Daofu-Kangding segment is about 0.003-0.01 MPa by using Wang and Yao's model, but is about 0.01-0.03 MPa by Ji and Hayes's model. The length of the positively stressed segment by Wang and Yao's model is a little longer than that by Ji and Hayes's model near the junction of XXFS and the Longmenshan fault. The Daofu-Kangding segment is the section A in Fig. 4 with high seismic hazard, which was also recognized to be the first seismic gap in the Xianshuihe fault zone by Wen et al. (2008). The combined stress change (co-, post-seismic stress change and tectonic loading) on the main part of this segment, which is about 125-km long, is larger than 1.2 MPa (Fig. 4b). Based on the empirical equation (Wells and Coppersmith, 1994), the increased stress caused by the Wenchuan earthquake further raises the probability of earthquake occurrence with magnitude up to Mw7.5. Considering the high population, earthquake monitoring and early warning system are especially needed in this region.

Due to the time-dependent stress transfer of post-seismic viscoelastic relaxation, the earthquake-trigger-earthquake process may keep up years to decades (Freed, 2001, 2005). Therefore, we calculate the stress evolution on the Daofu-Kangding segment caused by the Wenchuan earthquake by a multi-layer lithosphere model with rheological lower crust and upper mantle. As shown in Fig. 8, the snapshots on 1, 10 and 50 yr after the 2008 Wenchuan earthquake are calculated. The time-dependent stress transfer slightly raises the magnitude of stress accumulation on this segment in future 50 years, which does not influence significantly on the hazard assessment for the XXFS based on the historical seismicity.

## 5. Discussion and conclusions

Our analysis presents two improvements in relation to the previous work on the seismic hazard on the XXFS: (1) We consider a whole sequence of earthquakes on the entire XXFS in past

300 years instead of individual studies over the last century on Xianshuihe (Papadimitriou et al. 2004) and two centuries on Xiaojiang faults (Paradisopoulou et al. 2007). (2) We use a more realistic lithosphere structure to include the time-dependent effects of viscoelastic relaxation at the lower crust and upper mantle.

The co- and post-seismic stress triggering hypothesis is tested by using a sequence of 25 historical earthquakes along the XXFS and its stress evolution spanning the time interval from 1713 to 1981. The earthquake interaction analysis reveals that 15 out of 24 earthquakes posterior to the 1713 earthquake show potential encouragement effects due to the maximum cumulative ΔCFS values on the rupture surface. Furthermore, if the effect of post-seismic relaxation is included, 19 out of 24 earthquakes show potential encouragement due to the maximum ΔCFS values. Although the maximum ΔCFS for other 5 earthquakes are positive, but their magnitudes ($10^{-3}$~$10^{-4}$ MPa) are below the most assumed triggering threshold (0.01 MPa). Notice that these 5 earthquakes mainly occurred at the earlier period in our historical catalog, so that their pre-event stress state cannot be estimated reliably. From the cumulative ΔCFS on the XXFS, we can identify clearly four segments with significant CFS increment. These results are consistent with the seismic gaps given by the historical earthquake studies. Since the regions around these segments are highly populated, the seismic hazard in these areas is emphasized.

Analysis on the interaction between the historical earthquakes and the 2008 Wenchuan earthquake shows that the un-clamping normal stress changes at the hypocenter of the Mw7.9 earthquake are increased by the seismic activities and tectonic motion of the XXFS. However, the negative shear stress changes inhibit the occurrence of the Wenchuan earthquake at the same time interval. To sum up, the cumulative ΔCFS on the hypocenter is always negative, no matter how to choose the values of the effective coefficient of friction. Therefore, the seismic activities and tectonic motion the XXFS might not have encouraged the Wenchuan earthquake directly. On the other hand, the CFS increment induced by the Wenchuan earthquake positively stresses a 125-km-long segment of the XXFS at the northwest of Kangding City. Based on our model, the combined stress change (co-, post-seismic stress change and tectonic loading) on the main part of this segment has already accumulated at least to 1.2 MPa. The stress enhancement through the Wenchuan earthquake has further increased the current seismic hazard on this 125-km-long segment of the XXFS, which may generate empirically an earthquake of about Mw7.5.

Although our analysis considers co- and post- seismic stress changes, it is still suffered from some limitations. In particular, local effects could be produced by the oversimplified fault geometry and uniform slip distribution. Nevertheless, our results provide a quantitative view of the interaction among the earthquakes on the XXFS. Moreover, it should be mentioned that we have used the conventional stress-triggering model, in which only the total strength rather than the history of the stress loading is relevant. In principle, this model is only applicable to long-term hazard assessment. For short-term triggering sequences, the effect due to the stress loading history needs to be considered according to the rate and state dependent friction theory (Dieterich, 1994).

## Acknowledgments

We would like to thank the guest editor Peter Shearer and two anonymous reviewers for their insightful review and thoughtful comments that helped us greatly to improve the focus and quality of the manuscript. This work is supported by National Natural Science Foundation of China (Grant Nos. 41204067, 41074052, 41174086 and 41021003), Grant 201008007 from CEA , Key

Development Program of Chinese Academy of Sciences (Grant No. KZZD-EW-TZ-05) and CAS/SAFEA International Partnership Program for Creative Research Teams (Grant No. KZZD-EW-TZ-05). Figures were plotted with the Generic Mapping Tools (Wessel and Smith, 1998).

## References

Aki, K., Richards, P.G., 2002. Quantitative Seismology Second Edition, 73pp.University Science Books California, USA.

Ali, S.T., Freed, A.M., Calais, E., et al., 2008. Coulomb stress evolution in Northeastern Caribbean over the past 250 years due to coseismic, postseismic and interseismic deformation. Geophys. J. Int. 174, 904-918.

Allen, C.R., Luo, Z., Qian, H., et al., 1991. Field study of a highly active fault zone: the Xianshuihe fault of southwestern China. Geol. Soc. Am. Bull. 103, 1178-1199.

Chen, Z., Burchfiel, B.C., Liu, Y., et al., 2000. Global Positioning System measurements from eastern Tibet and their implications for India/Eurasia intercontinental deformation. J. Geophys. Res. 105(B7), 16215-16227.

Cohen, S.C., 1982. A multilayer model of time-dependent deformation following an earthquake on a strike-slip fault. J. Geophys. Res. 87, 5409-5421.

Deng, J., Hudnut, K., Gurnis, M., et al., 1999. Stress loading from viscous flow in the lower crust and triggering of aftershocks following the 1994 Northridge, California, earthquake. Geophys. Res. Lett. 26 (21), 3209-3212.

Deng, J., Sykes, L.R., 1996. Triggering of 1812 Santa Barbara earthquake by a great San Andreas shock: implications for future seismichazards in southern California. Geophys. Res. Lett. 23, 1155-1158.

Dieterich, J.H., 1994. A constitutive law for rate of earthquake production and its application to earthquake clustering, J. Geophys. Res. 99, 2601-2618.

Felzer, K.R., Brodsky, E.E., 2005. Testing the stress shadow hypothesis. J. Geophys. Res., 110, B05S09, doi: 10.1029/2004JB003277.

Felzer, K.R., Brodsky, E.E., 2006. Decay of aftershock density with distance indicates triggering by dynamic stress. Nature, 441, 735-738.

Freed, A.M., 2005. Earthquake triggering by static, dynamic and postseismic stress transfer. Annu. Rev. Earth Planet. Sci. 33, 335-367.

Freed, A.M., Ali, S.T., Bürgmann, R., 2007. Evolution of stress in Southern California for the past 200 years from coseismic, postseismic and interseismic stress changes. Geophys. J. Int. 169 (3), 1164-1179.

Freed, A.M., Lin, J., 2001. Delayed triggering of the 1999 Hector Mine earthquake by viscoelastic stress transfer. Nature 411 (6834), 180-183.

Harris, R.A., Simpson, R.W., Reasenberg, P.A., 1995. Influence of static stress changes on earthquake locations in southern California. Nature 375, 221-224.

Heidbach, O., Ben-Avraham, A., 2007. Stress evolution and seismic hazard of the Dead Sea fault system. Earth Planet. Sci. Lett. 257, 299-312.

Hodgkinson, K.M., Stein, R.S., Marshall, G., 1996. The 1954 Rainbow Mountain-Fairview Peak-Dixie Valley earthquake sequences: a triggered normal faulting sequence. J. Geophys. Res. 101, 25459-25472.

Holt, W.E., Ni, J.F., Wallace, T.C., et al., 1991. The active tectonics of the eastern Himalayan syntaxis and surrounding regions. J. Geophys. Res. 96(B9), 14595-14632.

Jaume, S.C., Sykes, L.R., 1996. Evolution of moderate seismicity in the San Francisco Bay region, 1850 to 1993: seismicity changes related to the occurrence of large and great earthquakes. J. Geophys. Res. 101, 765-789.

Ji, C., Hayes, G., 2008. Preliminary result of the May 12, 2008 Mw7.9 eastern Sichuan. http://earthquake.usgs.gov/eqcenter/eqinthenews/ 2008/us2008ryan/finite_fault.php.

King, G.C.P., Stein, R.S., Lin, J., 1994. Static stress changes and the triggering of earthquakes. Bull. Seismol. Soc. Am. 84, 935-953.

King, RW., Shen, F., Burchfiel, B.C., et al., 1997. Geodetic measurement of crustal motion in southwest China. Geology 25(2), 179-182.

Kirby, S.H., Kronenberg, A.K., 1987. Rheology of the lithosphere: Selected topics. Rev. Geophys. 25, 1219-1244.

Li, H.Y., Su, W., Wang, C.Y., et al., 2009. Ambient noise Rayleigh wave tomography in western Sichuan and eastern Tibet. Earth and Planetary Science Letters 282, 201-211.

Li, S.L., Mooney, W.D., 1998. Crustal structure of China from deep seismic sounding profiles. Tectonophysics 288, 105-113

Lin, J., Stein, R.S., 2004. Stress triggering in thrust and subduction earthquakes and stress interaction between the southern San Andreas and nearby thrust and strike-slip faults. J. Geophys. Res. 109, B02303, doi: 10.1029/2003JB002607

Liu, Q.Y., Li, Y., Chen, J.H., et al., 2009. Wenchuan Ms8.0 earthquake: preliminary study of the S-wave velocity structure of the crust and upper mantle. Chinese J. Geophys. 52(2), 309-319.

Lorenzo-Martín, F., Roth, F., Wang, R.J., 2006. Elastic and inelastic triggering of earthquakes in the North Anatolian Fault zone. Tectonophysics 424, 271-289.

Luo, G., Liu, M., 2010. Stress evolution and fault interactions before and after the 2008 Great Wenchuan earthquake. Tectonophysics doi:10.1016/j.tecto.2009.12.019.

Ma, K.F., Chan, C.H., Stein, R.S., 2005. Response of seismicity to Coulomb stress triggers and shadows of the 1999 Mw = 7.6 Chi-Chi, Taiwan, earthquake. J. Geophys. Res. 110, B05S19. doi:10.1029/2004JB003389.

Martínez-Díaz, J.J., Capote, R., Tsige, M., et al., 2006. Seismic triggering in a stable continental area: the Lugo 1995-1997 seismic sequences (NW Spain). J. Geodyn. 41, 440-449.

McCloskey, J., Nalbant, S.S., Steacy, S., 2005. Earthquake risk from co-seismic stress. Nature, 434 (7031), 291.

Molnar, P., Deng, Q.D., 1984. Faulting associated with large arthquakes and the average rate of deformation in central and eastern Asia. J. Geophys. Res. 89, 6203-6227.

Molnar, P., Lyon-Caen, H., 1989. Fault plane solutions of earthquakes and active tectonics of the Tibetan Plateau and its margins. Geophys. J. Int. 99, 123-153.

Molnar, P., Tapponnier, P., 1975. Cenozoic tectonics of Asia: effects of a continental collision. Science 189(4201), 419-426.

Nalbant, S.S., Hubert, A., King, G.C.P., 1998. Stress coupling between earthquakes in northwest Turkey and the north Aegean Sea. J. Geophys. Res. 103, 24 469-24486.

Nalbant, S.S., Steacy, S., McCloskey, J., et al., 2005. Earthquake risk on the Sunda trench. Nature 435 (7043), 756-757.

Papadimitriou, E., Wen, X.Z., Karakostas, V., et al., 2004. Earthquake triggering along the Xianshuihe Fault zone of western Sichuan, China. Pure appl. Geophys. 161, 1683-1707.

Paradisopoulou, P.M., Garlaouni, C.G., Jin, X.S., et al., 2007. Application of the stress evolutionary model along the Xiaojiang fault zone in Yunnan Province, Southeast China. Acta Geophysica 55(4), 577-593.

Parsons, T., Chen, J., Kirby, E., 2008. Stress changes from the 2008 Wenchuan earthquake and increase hazard in the Sichuan basin. Nature 454, 509-510.

Parsons, T., Stein, R.S., Simpson, R.W., et al., 1999. Stress sensitivity of fault seismicity: a comparison between limited-offset oblique and major strike-slip faults. J. Geophys. Res. 104, 20183-20202.

Pollitz, F.F., Burgmann, R., Segall, p., 1998. Joint estimation of afterslip rate and postseismic relaxation following the 1989 Loma Prieta earthquake. J. Geophys. Res. 103(B11), 26975-26992.

Pollitz, F., Vergnolle,M., Calais, E., 2003. Fault interaction and stress triggering of twentieth century earthquakes in Mongolia. J. Geophys. Res. 108 (B10), 2503. doi:10.1029/002JB002375.

Pollitz, F.F., Wicks, C., Thatcher, W., 2001. Mantle flow beneath a continental strike-slip fault: postseismic deformation after the 1999 Hector earthquake. Science 293(5536), 1814-1818.

Reasenberg, P.A., Simpson, R.W., 1992. Response of regional seismicity to the static stress change produced by the Loma Prieta earthquake. Science 255, 1687-1690.

Richards-Dinger, K., Stein, R.S., Toda, S., 2010. Decay of aftershock density with distance does not indicate triggering by dynamic stress. Nature, 2010, 467, 583-586.

Savage, J.C., 1983. A dislocation model of strain accumulation and release at a subduction zone. J. Geophys. Res. 88, 4984-4996.

Scholz, C.H., 1990. The Mechanics of Earthquakes and Faulting. Cambridge Univ. Press, New York, p. 439.

Shen, Z.K., Lv, J.N., Wang, M., et al., 2005. Contemporary crustal deformation around the southeast borderland of the Tibetan Plateau. J. Geophys. Res. 110, B11409, doi: 10.1029/2004JB003421.

Shan, B., Xiong, X., Zheng, Y., et al., 2009. Stress changes on major faults caused by Mw7.9 Wenchuan earthquake, May 12, 2008. Sci. China Ser. D-Earth Sci. 52(5), 593-601.

Shi, Y.L., Cao, J.L., 2008. Lithosphere effective viscosity of continental China. Earth Science Frontiers 15(3), 82-95.

Smith, B.R., Sandwell, D.T., 2006. A model of the earthquake cycle along the San Andreas Fault System for the past 1000 years. J. Geophys. Res. 111, B01405, doi: 10.1029/2005JB03703.

Song, F., Wang, Y., Yu, W., et al., 1998. The active Xiaojiang fault Zone. Seismological Press, Beijing, 237pp. (in Chinese)

Stein, R.S., 1999. The role of stress transfer in earthquake occurrence. Nature 402, 605-609.

Stein, R.S., 2003. Earthquake conversations. Scient. Am. 288, 72-79.

Stein, R.S., Barka, A.A., Dieterich, J.H., 1997. Progressive failure on the North Anatolian fault since 1939 by earthquake stress triggering. Geophys. J. Int. 128, 594-604.

Stein, R.S., King, G.C.P., Lin, J., 1994. Stress triggering of the 1994 M = 6.7 Northridge, California, earthquake by its predecessors. Science 265 (5177), 1432-1435.

Toda, S., Lin, J., Meghraoui, M., et al., 2008. 12 May 2008 M=7.9 Wenchuan, China, earthquake alculated to increase failure stress and seismicity rate on three major fault systems. Geophys. Res. Lett. 35, L17305, doi: 10.1029/2008GL034903.

Toda, S., Stein, R.S., Reasenberg, P.A., et al., 1998. Stress transferred by the Mw=6.5 Kobe, Japan, shock: effect on aftershocks and future earthquake probabilities. J. Geophys. Res. 103, 24543-24565.

Wang, E., Burchfiel, B.C., 2000. Late Cenozoic to Holocene deformation in southwestern Sichuan and adjacent Yunnan, China, and its role in formation of the southeastern part of the Tibetan Plateau. Geol. Soc. Am. Bull. 112(3), 413-423.

Wang, R., Lorenzo Martín, F., Roth, F., 2003. Computation of deformation induced by earthquakes in a multi-layered elastic crust — FORTRAN programs EDGRN/EDCMP. Comput. Geosci. 29 (2), 195-207.

Wang, R., Lorenzo-Martín, F., Roth, F., 2006. PSGRN/PSCMP-a new code for calculating co- and post-seismic deformation, geoid and gravity changes based on the viscoelastic- gravitational dislocation theory. Comput. Geosci. 32527-32541.

Wang, W., Zhao, L., Li, J., et al., 2008. Rupture process of the Ms 8.0 Wenchuan earthquake of Sichuan, China. *Chin. J. Geophys.* 51:1403–1410.

Wells, D.L., Coppersmith, K.J., 1994. New empirical relationships among magnitude, rupture length, rupture width, rupture area, and surface displacement. Bull. Seism. Soc. Am., 84, 974-1002.

Wen, X., Ma, S., Lei, X., et al., 2007. Newly found surface rupture remains of large historical earthquakes on and near the transition segment of the Anninghe and Zemuhe fault zones,western Sichuan, China. Seismol. Geol. 29, 826–833 (in Chinese).

Wen, X.Z., Ma, S.L., Xu, X.W., et al., 2008. Historical pattern and behavior of earthquake ruptures along the eastern boundary of the Sichuan-Yunan faulted-block, southwestern China. Physics of the Earth and Planetary Interiors 168, 16-36.

Wen, Y., Li, Z., Xu, C., et al., 2012. Postseismic motion after the 2001 Mw 7.8 Kooxili earthquake in Tibet observed by InSAR time seris. J. Geophys. Res. 117, B08405, doi:10.1029/2011JB009043.

Wessel, P., Smith, W.H.F., 1998. New improved version of Generic Mapping Tools released, Eos, Trans. Am. Geophys. Union 79:579.

Wyss, M., Wiemer, S., 2000. Change in the probability for earthquakes in southern California due to the Landers magnitude 7.3 earthquake. Science, 290, 1334-1338.

Xiong, X., Shan, B., Zheng, Y., et al., 2010. Stress transfer and its implication for earthquake hazard on the Kunlun Fault, Tibet. Tectonophysics 482, 216-225.

Xu, X., Wen, X., Zheng, R., et al., 2003. Pattern of latest tectonic motion and its dynamics for active blocks in Sichuan-Yunnan region, China. Sci. China (Series D) 46 (Suppl.), 210-226.

Zhang, P.Z., Shen, Z.K., Wang, M., et al., 2004. Continuous deformation of the Tibetan Plateau from global positioning system data. Geology 32(9), 809-812.

Zhang, P.Z., Wen, X.Z., Shen, Z.K., et al., 2010. Oblique, high-angle, listric-reverse faulting and associated development of strain: the Wenchuan earthquake of May 12, 2008, Sichuan, China. Annu. Rev. Earth. Planet. Sci. 38, 353-382

Zhang, X., Wang, Y.H., 2009. Crustal and upper mantle velocity structure in Yunnan, Southwest China. Tectonophysics 471(3-4), 171-185.

Zhou, H.L., Allen, C.R., Knamori, H., 1983a. Rupture complexity of the 1970 Tonghai and 1973 Luhuo earthquakes, China, from P-wave inversion, and Relationship to surface faulting. Bull. Seismol. Soc. Am. 73, 1585-1597.

Zhou, H.L., Liu, H.L., Kanamori, H., 1983b. Source processes of large earthquakes along the Xianshuihe fault in southwestern China. Bull. Seismol. Soc. Am. 73, 537-551.

**Figure caption**

Fig. 1. Location map of the Xianshuihe-Xiaojiang Fault System (XXFS) and the space distribution of 25 M≥6.5 earthquakes along the XXFS during the period 1713 to 1966. The focal mechanisms with serial number are listed in table 1. Colorful lines show the slip rate of the XXFS. The symbols represent the locations and populations of cities (downward solid triangle: population <0.1 million; upward solid triangle: 0.1-0.5 million; solid square: 0.5-1 million; solid circle: >1 million). Inset shows the location of the study region in the whole China.

Fig. 2. Stratified model comprised of elastic upper crust, viscoelastic lower crust and viscoelastic mantle. $V_P$ is the velocity of $P$ wave. $\mu$ is the shear modulus. $\rho$ is the rock density, and $\eta$ is viscosity ($\eta_{LC}$, lower crustal viscosity; $\eta_M$, mantle viscosity). $\eta_{LC}$ and $\eta_M$ are set to be $1\times10^{19}$ and $1\times10^{20}$ Pa·s , respectively. Other values of viscosities are used for comparison and stability tests.

Fig. 3. Stress evolution along the XXFS fault due to earthquake interactions since 1713. Each subfigure describes the cumulative CFS on the fault segment of one of 6 typical earthquake (labelled with the occurrence year in black and white). Dashed and solid lines of the same colour represent the stress state along the segment before and after the occurrence of one of the 25 major earthquakes (labelled with the occurrence year in the same colour as the corresponding stress curves), respectively, which has a significant influence on the current one.

Fig. 4. Coulomb failure stress state of the XXFS in the year of 2010. Displayed are the cumulative ΔCFS since 1713 calculated for the varying orientation of each fault in 1-km step. The ΔCFS values (a) include co- and post-seismic stress changes; and (b) combined stress change (co-, post-seismic stress change and tectonic loading). Units A-D are the four segments on which cumulative ΔCFS is positive. Yellow circles are cities with population larger than 1 million. The signals S1-S14 by the left side of XXFS are the segments given by Wen et al. (2008).

Fig. 5. Current stress accumulation for four main fault segments with high stress increment since 1713 along the XXFS. The signals in the right upper corner as shown in Fig. 4 indicate the location of these segments. To illuminate the different contributions of co-, post- and inter-seismic stress transfer to the process of stress evolution, lines in different colors indicate different cumulative CFS compositions: Green, black and blue solid lines indicate the co-, post-seismic Coulomb stress changes and interseismic tectonic loading,

respectively. Red and purple solid line indicate the combined stress change (red: co- and post-seismic ΔCFS; purple: co-, post-seismic ΔCFS and tectonic loading)

Fig. 6 Evolution of the cumulative stress on the hypocenter of Mw7.9 Wenchuan earthquake during the time interval from 1713 (ΔCFS=0) to 2008. The solid and dash lines represent the stress changes on the two proposed focal depths of 14.5 km (Zhang, 2010) and 19 km (Liu et al., 2009). Lines in red and green represent the shear and normal stress evolution on the hypocenter of Wenchuan earthquake. Lines in blue and black color represent the CFS evolution results with different effective coefficient of friction, 0.6 and 0.8, respectively.

Fig. 7. Cumulative ΔCFS on the XXFS caused by the Mw7.9 Wenchuan earthquake with different slip model (a) Ji and Hayes (2008); and (b) Wang et al. (2008). Red star represents the epicenter of Mw7.9 Wenchuan earthquake. Black boxes represent the surface projection of rupture plane of Wenchuan earthquake. Yellow circles are cities with population over 1 million.

Fig. 8. The snapshots of ΔCFS accumulation on the XXFS caused by the Mw7.9 Wenchuan earthquake with time intervals of (a) 1 year, (b) 10 years, (c) 50 years after the 2008 earthquake. The symbols are the same as Fig. 7.

Table 1

Model parameters for the historical earthquakes

| *No.* | *Data* *YYYY-MO-DY* | *Magnitude* | *Central Coordinates* | | *Strike/Dip/Rake* | *Length* *(km)* | *Width* *(km)* | *Slip* *(m)* | *Ref* |
|---|---|---|---|---|---|---|---|---|---|
| | | | Latitude | Longitude | | | | | |
| | Xianshuihe fault zone | | | | | | | | |
| 1 | 1725-08-01 | 7 | 30.16°N | 101.83°E | 140°/80°/0° | 50 | 13.5 | 0.70 | 1, 2 |
| 2 | 1747-03 | 6.75 | 31.23°N | 100.85°E | 145°/90°/0° | 30 | 11.5 | 0.47 | 1, 2 |
| 3 | 1748-08-30 | 6.5 | 30.33°N | 101.62°E | 135°/85°/0° | 35 | 9.9 | 0.16 | 1, 2 |
| 4 | 1786-06-01 | 7.75 | 29.87°N | 102.04°E | 170°/80°/0° | 90 | 21.5 | 5.70 | 1, 2 |
| 5 | 1792-09-07 | 6.75 | 31.06°N | 101.00°E | 145°/90°/0° | 25 | 11.5 | 0.57 | 1, 2 |
| 6 | 1811-09-27 | 6.75 | 31.61°N | 100.15°E | 245°/45°/42° | 15 | 11.5 | 0.95 | 1, 2 |
| 7 | 1816-12-08 | 7.5 | 31.29°N | 100.75°E | 145°/90°/0° | 60 | 18.4 | 3.52 | 1, 2 |
| 8 | 1893-08-29 | 7 | 30.70°N | 101.37°E | 322°/85°/13° | 70 | 13.5 | 0.50 | 1, 2 |
| 9 | 1904-08-30 | 7 | 31.06°N | 101.00°E | 322°/85°/13° | 55 | 13.5 | 0.64 | 1, 2 |
| 10 | 1923-03-24 | 7.3 | 31.17°N | 100.90°E | 306°/90°/0° | 60 | 16.3 | 1.73 | 1, 2, 4 |
| 11 | 1955-04-14 | 7.5 | 30.03°N | 101.84°E | 340°/90°/0° | 35 | 18.4 | 6.04 | 1, 2, 4 |
| 12 | 1967-08-30 | 6.8 | 31.62°N | 100.20°E | 245°/45°/42° | 18 | 11.9 | 0.95 | 1, 2, 5 |
| 13 | 1973-02-06 | 7.6 | 31.50°N | 100.52°E | 125°/87°/0° | 90 | 19.6 | 3.35 | 1, 2, 4 |
| 14 | 1981-01-24 | 6.9 | 30.95°N | 101.15°E | 321°/90°/0° | 45 | 12.7 | 0.55 | 1, 2, 4 |
| | Anninghe fault zone | | | | | | | | |
| 15 | 1732-01-29 | 6.75 | 27.38°N | 102.52°E | 150°/60°/0° | 45 | 11.5 | 0.32 | 1, 2 |
| 16 | 1850-09-12 | 7.5 | 27.37°N | 102.53°E | 150°/60°/0° | 110 | 18.4 | 1.92 | 1, 2 |
| 17 | 1952-09-30 | 6.75 | 28.41°N | 102.18°E | 0°/75°/0° | 40 | 11.5 | 0.36 | 1, 2 |
| | Xiaojiang fault zone | | | | | | | | |
| 18 | 1713-02-26 | 6.75 | 25.47°N | 103.24°E | 10°/80°/0° | 60 | 11.5 | 0.24 | 1, 3 |
| 19 | 1725-01-08 | 6.75 | 25.13°N | 103.04°E | 45°/80°/0° | 50 | 11.5 | 0.28 | 1, 3 |
| 20 | 1733-08-02 | 7.75 | 26.37°N | 103.09°E | 345°/80°/0° | 110 | 21.5 | 4.66 | 1, 3 |
| 21 | 1763-12-30 | 6.5 | 24.25°N | 102.94°E | 20°/80°/0° | 40 | 9.9 | 0.14 | 1, 3 |
| 22 | 1789-06-07 | 7 | 24.29°N | 102.96°E | 14°/80°/0° | 60 | 13.5 | 0.59 | 1, 3 |
| 23 | 1833-09-06 | 8 | 25.00°N | 103.00°E | 15°/80°/0° | 130 | 25.1 | 9.50 | 1, 3 |
| 24 | 1909-05-11 | 6.5 | 24.35°N | 103.15°E | 10°/80°/0° | 40 | 9.9 | 0.14 | 1, 3 |
| 25 | 1966-02-05 | 6.5 | 26.10°N | 103.15°E | 345°/80°/0° | 45 | 9.9 | 0.13 | 1, 3 |

The width of rupture and amount of slip is estimated by the empirical scaling laws and relationships of Wells and Coppersmith (1994).

Ref: the references in the Table 1 that the relevant parameters of earthquake ruptures are derived from are listed below,

1. Wen, et al., 2008; 2. Papadimitriou, et al., 2004; 3. Paradisopoulou, et al., 2004; 4. Molnar, 1984; 5. Molnar, 1989.

Table 2

Maximum and average Coulomb stress changes (ΔCFS) on the rupture fault at the occurrence time of the event

| *Year* | *Co-Seismic Stress Changes* | | | | | *Co- & Post-Seismic Stress Changes* | | | | |
|---|---|---|---|---|---|---|---|---|---|---|
| | Encouraged | Max (MPa) | Encouraged | Mean (MPa) | P (%) | Encouraged | Max (MPa) | Encouraged | Mean (MPa) | P (%) |
| 1713 | | | | | | | | | | |
| 1725a | － | 0.009 | － | -0.025 | 0.0 | ＋ | 0.020 | － | -0.010 | 56.9 |
| 1725b | － | 0 | － | 0 | 0.0 | － | $1\times10^{-4}$ | － | $1\times10^{-4}$ | 0.0 |
| 1732 | － | $3\times10^{-4}$ | － | $2\times10^{-4}$ | 0.0 | － | $1.7\times10^{-3}$ | － | $1.1\times10^{-3}$ | 0.0 |
| 1733 | － | $4.0\times10^{-3}$ | － | $-4\times10^{-4}$ | 0.0 | － | $7.2\times10^{-3}$ | － | $-2.1\times10^{-3}$ | 0.0 |
| 1747 | － | $1.5\times10^{-3}$ | － | $1.1\times10^{-3}$ | 0.0 | － | $8.0\times10^{-3}$ | － | $6.4\times10^{-3}$ | 0.0 |
| 1748 | ＋ | 0.784 | － | -0.315 | 52.8 | ＋ | 0.967 | － | -0.163 | 58.3 |
| 1763 | － | 0.003 | － | 0.002 | 0.0 | ＋ | 0.042 | ＋ | 0.036 | 100.0 |
| 1786 | ＋ | 5.317 | ＋ | 0.075 | 63.7 | ＋ | 5.321 | ＋ | 0.098 | 65.9 |
| 1789 | ＋ | 0.390 | － | -0.121 | 32.8 | ＋ | 0.455 | － | -0.048 | 36.1 |
| 1792 | ＋ | 1.221 | ＋ | 0.038 | 84.6 | ＋ | 1.332 | ＋ | 0.110 | 84.6 |
| 1811 | － | $-1\times10^{-4}$ | － | $-1.1\times10^{-3}$ | 0.0 | － | $1.6\times10^{-3}$ | － | $-3.2\times10^{-3}$ | 0.0 |
| 1816 | ＋ | 0.253 | － | -0.278 | 36.1 | ＋ | 0.374 | － | -0.152 | 45.9 |
| 1833 | ＋ | 0.045 | － | -0.074 | 12.2 | ＋ | 0.292 | ＋ | 0.080 | 80.9 |
| 1850 | ＋ | 0.487 | － | -0.030 | 55.0 | ＋ | 1.022 | ＋ | 0.234 | 66.7 |
| 1893 | ＋ | 0.155 | ＋ | 0.072 | 85.9 | ＋ | 0.464 | ＋ | 0.342 | 100.0 |
| 1904 | ＋ | 3.516 | － | -2.031 | 25.0 | ＋ | 4.060 | － | -1.103 | 39.3 |
| 1909 | ＋ | 0.069 | － | -1.406 | 2.4 | ＋ | 1.825 | － | -0.061 | 26.8 |
| 1923 | ＋ | 0.384 | － | -3.255 | 4.9 | ＋ | 1.345 | － | -1.755 | 21.3 |
| 1952 | ＋ | 0.035 | ＋ | 0.029 | 100.0 | ＋ | 0.185 | ＋ | 0.168 | 100.0 |
| 1955 | － | -0.723 | － | -3.268 | 0.0 | ＋ | 0.344 | － | -1.577 | 8.3 |
| 1966 | ＋ | 1.862 | － | -4.939 | 6.5 | ＋ | 3.667 | － | -2.568 | 8.7 |
| 1967 | ＋ | 0.061 | － | -0.089 | 15.8 | ＋ | 0.145 | － | -0.043 | 42.1 |
| 1973 | ＋ | 2.451 | － | -2.043 | 47.3 | ＋ | 3.641 | － | -0.913 | 52.7 |
| 1981 | － | -0.180 | － | -1.633 | 0.0 | ＋ | 1.012 | － | -0.397 | 50.0 |

P (%) indicates the percentage of the rupture length with ΔCFS≥ 0.01MPa. ‘＋’ significant encouragement due to the preceding earthquakes assuming a threshold value of mean/maximum ΔCFS ≥ 0.01MPa on rupture plane; ‘－’: ΔCFS < 0.01MPa.

Table 3

Percentage of fault rupture showing ΔCFS ≥ 0.01MPa with different effective coefficient of friction and viscosities of lower crust and upper mantle

| *Year* | *Percentage of ΔCFS≥ 0.01MPa on the Rupture (%)* | | | | | | | | | | | |
|---|---|---|---|---|---|---|---|---|---|---|---|---|
| | Co-Seismic | | | Co- & Post-Seismic | | | $\rho_m=1\times10^{20}$ (Pa·s) | | | $\rho_c=1\times10^{18}$ (Pa·s) | | |
| | μ'=0.2 | μ'=0.4 | μ'=0.6 | μ'=0.2 | μ'=0.4 | μ'=0.6 | $\rho_c=10^{17}$ | $\rho_c=10^{18}$ | $\rho_c=10^{19}$ | $\rho_m=10^{18}$ | $\rho_m=10^{19}$ | $\rho_m=10^{20}$ |
| 1713 | | | | | | | | | | | | |
| 1725a | 0.0 | 0.0 | 0.0 | 56.9 | 56.9 | 54.9 | 56.9 | 56.9 | 31.4 | 56.9 | 56.9 | 56.9 |
| 1725b | 0.0 | 0.0 | 0.0 | 0.0 | 0.0 | 0.0 | 0 | 0.0 | 0.0 | 0.0 | 0.0 | 0.0 |
| 1732 | 0.0 | 0.0 | 0.0 | 0.0 | 0.0 | 0.0 | 0 | 0.0 | 0.0 | 0.0 | 0.0 | 0.0 |
| 1733 | 0.0 | 0.0 | 0.0 | 0.0 | 0.0 | 0.0 | 0 | 0.0 | 0.0 | 0.0 | 0.0 | 0.0 |
| 1747 | 0.0 | 0.0 | 0.0 | 0.0 | 0.0 | 0.0 | 0.0 | 0.0 | 0.0 | 0.0 | 0.0 | 0.0 |
| 1748 | 50.0 | 52.8 | 55.5 | 58.3 | 58.3 | 61.1 | 58.3 | 58.3 | 58.3 | 58.3 | 58.3 | 58.3 |
| 1763 | 0.0 | 0.0 | 0.0 | 100.0 | 100.0 | 100.0 | 100.0 | 100.0 | 82.9 | 100.0 | 100.0 | 100.0 |
| 1786 | 65.9 | 63.7 | 62.6 | 65.9 | 65.9 | 70.3 | 65.9 | 65.9 | 65.9 | 65.9 | 65.9 | 65.9 |
| 1789 | 31.1 | 32.8 | 32.8 | 34.4 | 36.1 | 39.3 | 36.1 | 36.1 | 34.4 | 36.1 | 36.1 | 36.1 |
| 1792 | 84.6 | 84.6 | 84.6 | 84.6 | 84.6 | 88.5 | 84.6 | 84.6 | 84.6 | 84.6 | 84.6 | 84.6 |
| 1811 | 0.0 | 0.0 | 0.0 | 0.0 | 0.0 | 31.2 | 0.0 | 0.0 | 0.0 | 0.0 | 0.0 | 0.0 |
| 1816 | 34.4 | 36.1 | 37.7 | 42.6 | 45.9 | 47.5 | 45.9 | 45.9 | 45.9 | 45.9 | 45.9 | 45.9 |
| 1833 | 8.4 | 12.2 | 20.6 | 80.9 | 80.9 | 78.6 | 81.7 | 80.9 | 67.9 | 82.5 | 81.7 | 80.9 |
| 1850 | 53.2 | 55.0 | 56.7 | 66.7 | 66.7 | 65.8 | 77.5 | 66.7 | 60.3 | 73.0 | 69.4 | 66.7 |
| 1893 | 88.7 | 85.9 | 84.5 | 100.0 | 100.0 | 100.0 | 100.0 | 100.0 | 100.0 | 100.0 | 100.0 | 100.0 |
| 1904 | 25.0 | 25.0 | 25.0 | 41.1 | 39.3 | 37.5 | 41.1 | 39.3 | 32.1 | 42.0 | 41.1 | 39.3 |
| 1909 | 0.0 | 2.4 | 14.6 | 19.5 | 26.8 | 31.7 | 26.8 | 26.8 | 24.4 | 26.8 | 26.8 | 26.8 |
| 1923 | 3.2 | 4.9 | 9.8 | 21.3 | 21.3 | 21.3 | 21.3 | 21.3 | 19.7 | 21.3 | 21.3 | 21.3 |
| 1952 | 100.0 | 100.0 | 100.0 | 100.0 | 100.0 | 100.0 | 100.0 | 100.0 | 100.0 | 100.0 | 100.0 | 100.0 |
| 1955 | 0.0 | 0.0 | 0.0 | 5.6 | 8.3 | 11.1 | 8.3 | 8.3 | 8.3 | 8.3 | 8.3 | 8.3 |
| 1966 | 6.5 | 6.5 | 6.5 | 8.7 | 8.7 | 8.7 | 8.7 | 8.7 | 8.7 | 8.7 | 8.7 | 8.7 |
| 1967 | 10.5 | 15.8 | 52.6 | 15.8 | 42.1 | 57.8 | 42.1 | 42.1 | 37.9 | 42.1 | 42.1 | 42.1 |
| 1973 | 46.2 | 47.3 | 46.1 | 50.5 | 52.7 | 51.6 | 52.7 | 52.7 | 52.7 | 52.7 | 52.7 | 52.7 |
| 1981 | 0.0 | 0.0 | 2.2 | 47.8 | 50.0 | 47.8 | 50.0 | 50.0 | 39.1 | 50.0 | 50.0 | 50.0 |

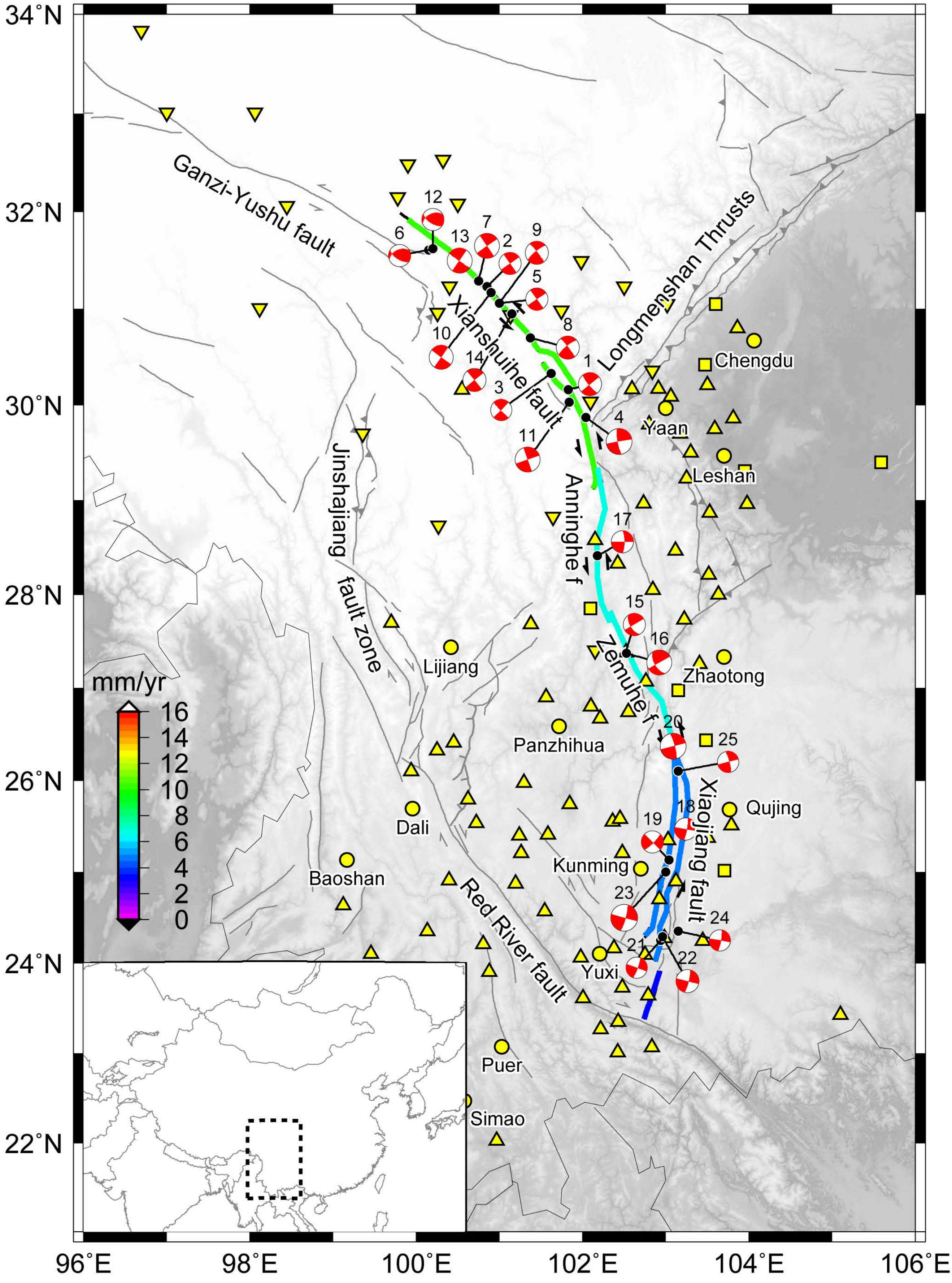

34°N
32°N
30°N
28°N
26°N
24°N
22°N
96°E
98°E
100°E
102°E
104°E
106°E
Ganzi-Yushu fault
Xianshuihe fault
Longmenshan Thrusts
Jinshajiang fault zone
Anninghe f
Zemuhe f
Xiaojiang fault
Red River fault
Chengdu
Yaan
Leshan
Lijiang
Zhaotong
Panzhihua
Qujing
Dali
Kunming
Baoshan
Yuxi
Puer
Simao
mm/yr
16
14
12
10
8
6
4
2
0
1
2
3
4
5
6
7
8
9
10
11
12
13
14
15
16
17
18
19
20
21
22
23
24
25

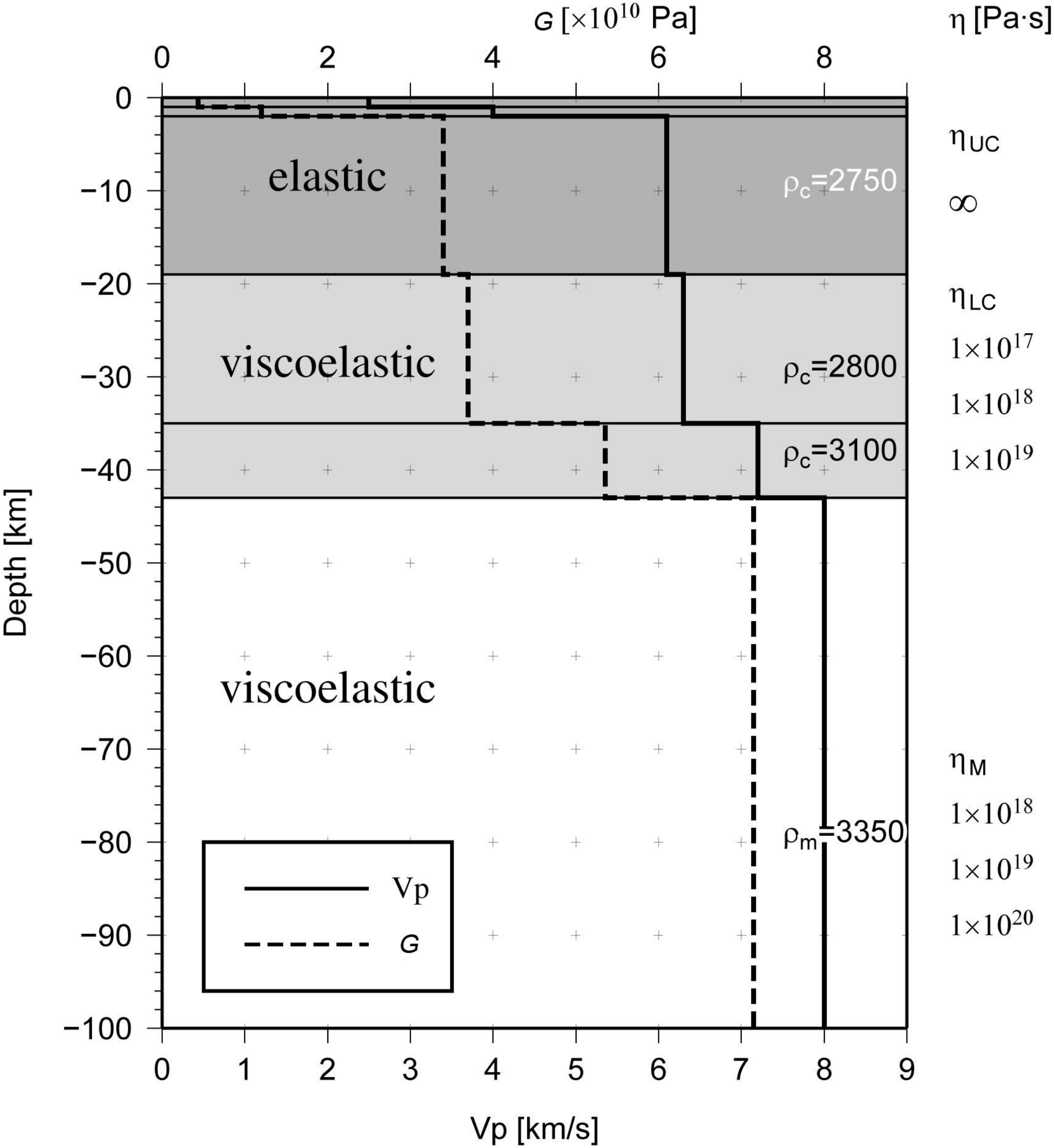

G [×10^10 Pa]
η [Pa·s]
0
2
4
6
8
elastic
viscoelastic
viscoelastic
ρc=2750
ρc=2800
ρc=3100
ρm=3350
ηUC
∞
ηLC
1×10^17
1×10^18
1×10^19
ηM
1×10^18
1×10^19
1×10^20
Vp
G
Depth [km]
0
−10
−20
−30
−40
−50
−60
−70
−80
−90
−100
0
1
2
3
4
5
6
7
8
9
Vp [km/s]

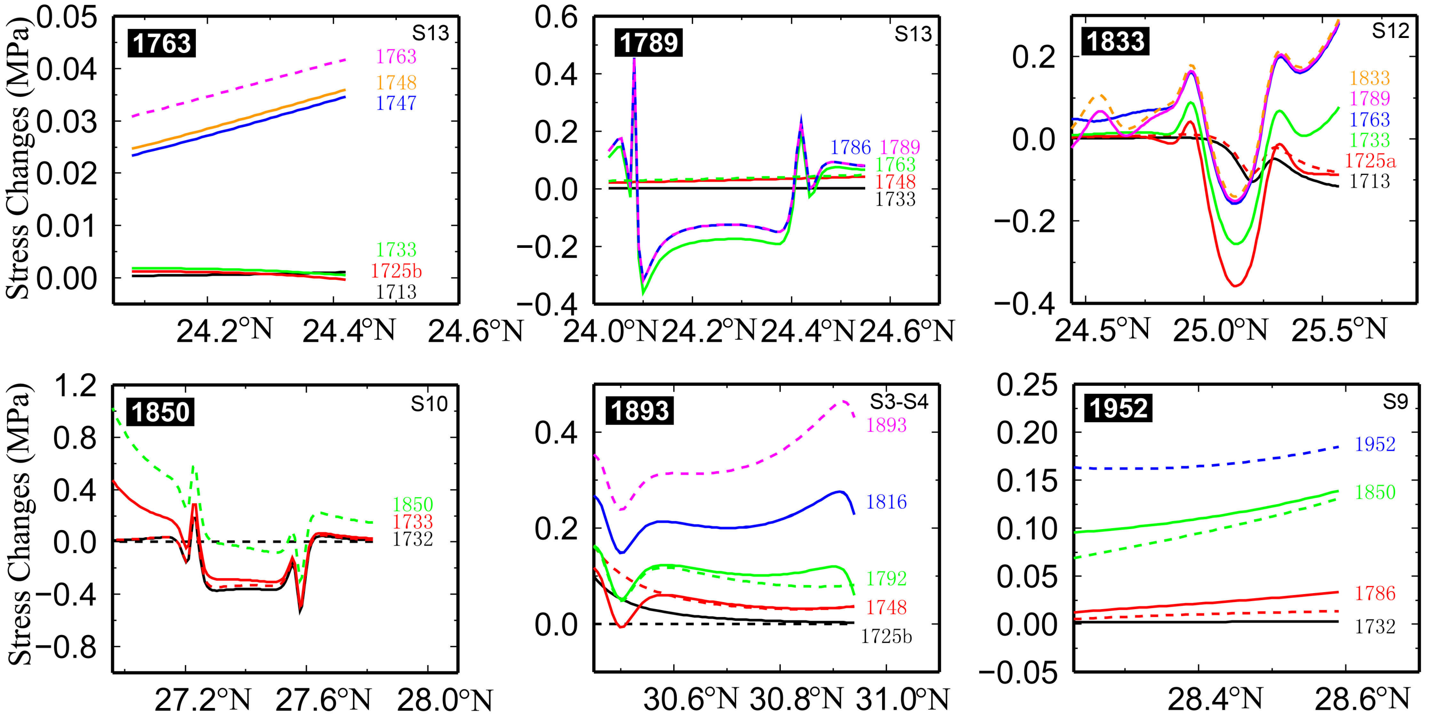

Stress Changes (MPa)
1763
S13
1763
1748
1747
1733
1725b
1713
0.05
0.04
0.03
0.02
0.01
0.00
24.2°N
24.4°N
24.6°N
1789
S13
1786 1789
1763
1748
1733
0.6
0.4
0.2
0.0
−0.2
−0.4
24.0°N
24.2°N
24.4°N
24.6°N
1833
S12
1833
1789
1763
1733
1725a
1713
0.2
0.0
−0.2
−0.4
24.5°N
25.0°N
25.5°N
Stress Changes (MPa)
1850
S10
1850
1733
1732
1.2
0.8
0.4
0.0
−0.4
−0.8
27.2°N
27.6°N
28.0°N
1893
S3-S4
1893
1816
1792
1748
1725b
0.4
0.2
0.0
30.6°N
30.8°N
31.0°N
1952
S9
1952
1850
1786
1732
0.25
0.20
0.15
0.10
0.05
0.00
−0.05
28.4°N
28.6°N

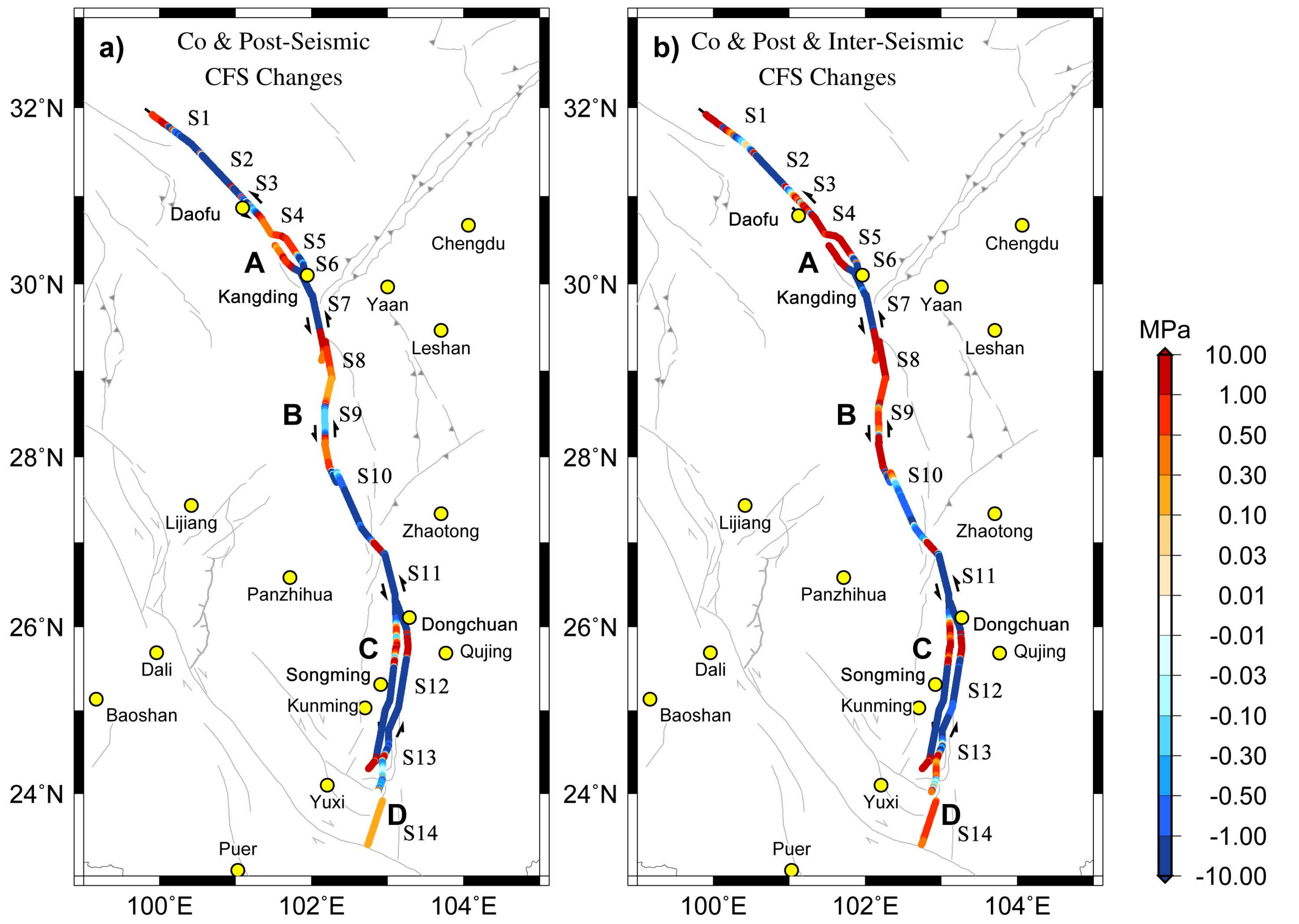
a)
Co & Post-Seismic
CFS Changes
b)
Co & Post & Inter-Seismic
CFS Changes
32°N
30°N
28°N
26°N
24°N
100°E
102°E
104°E
S1
S2
S3
S4
S5
S6
S7
S8
S9
S10
S11
S12
S13
S14
A
B
C
D
Daofu
Kangding
Chengdu
Yaan
Leshan
Lijiang
Zhaotong
Panzhihua
Dongchuan
Qujing
Dali
Songming
Kunming
Baoshan
Yuxi
Puer
MPa
10.00
1.00
0.50
0.30
0.10
0.03
0.01
-0.01
-0.03
-0.10
-0.30
-0.50
-1.00
-10.00

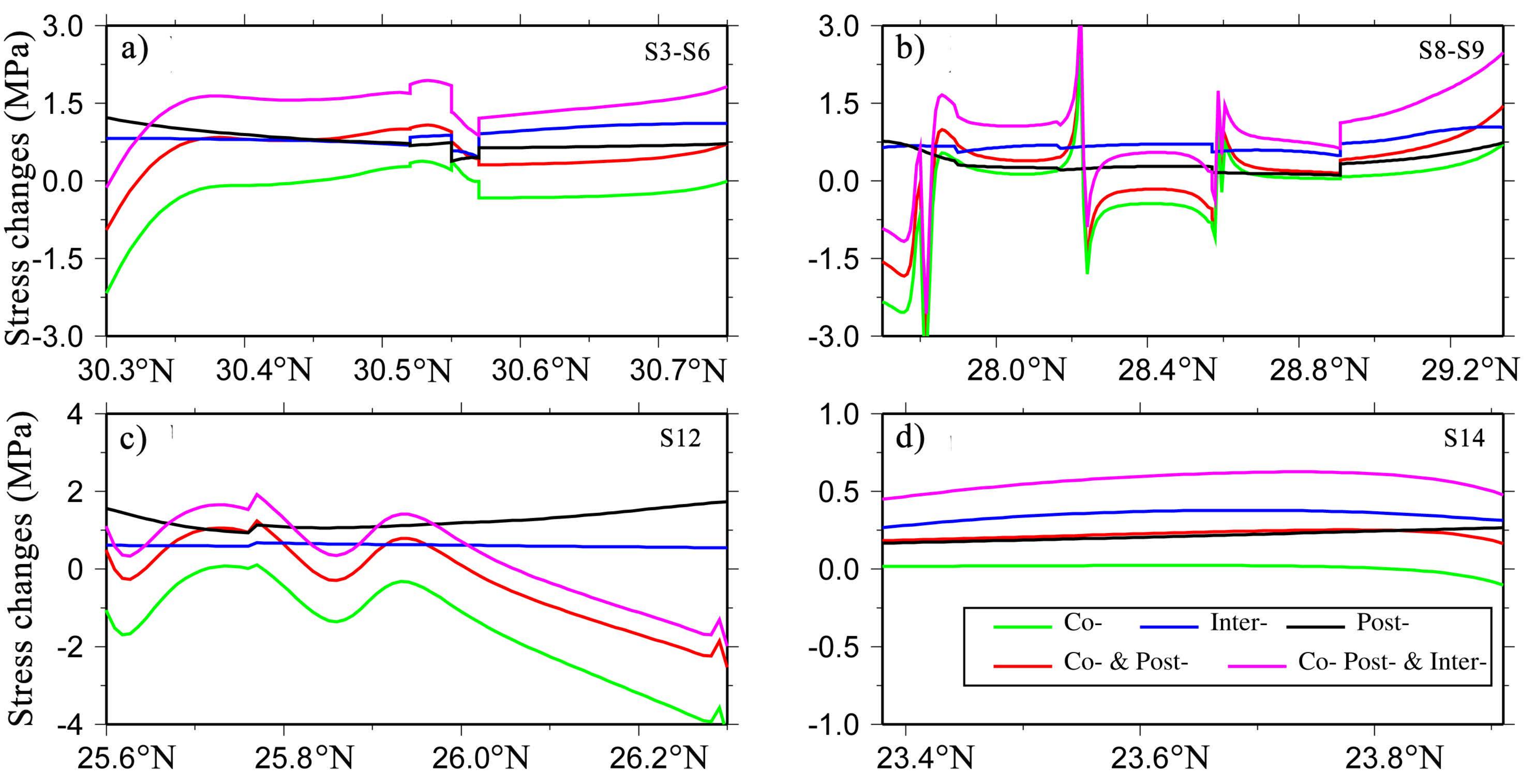

a)
S3-S6
b)
S8-S9
c)
S12
d)
S14
Stress changes (MPa)
Stress changes (MPa)
3.0
1.5
0.0
-1.5
-3.0
4
2
0
-2
-4
1.0
0.5
0.0
-0.5
-1.0
30.3°N
30.4°N
30.5°N
30.6°N
30.7°N
28.0°N
28.4°N
28.8°N
29.2°N
25.6°N
25.8°N
26.0°N
26.2°N
23.4°N
23.6°N
23.8°N
Co-
Inter-
Post-
Co- & Post-
Co- Post- & Inter-

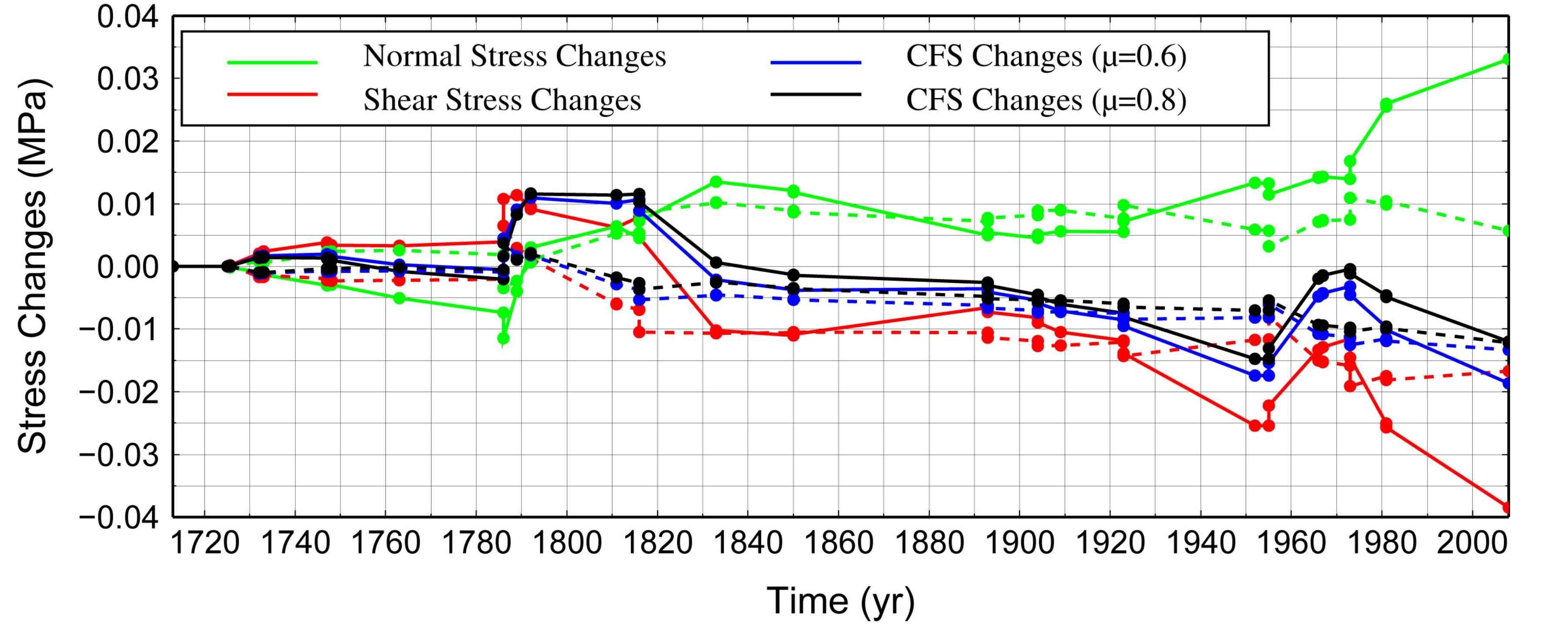

Normal Stress Changes
Shear Stress Changes
CFS Changes (μ=0.6)
CFS Changes (μ=0.8)
Stress Changes (MPa)
0.04
0.03
0.02
0.01
0.00
−0.01
−0.02
−0.03
−0.04
1720
1740
1760
1780
1800
1820
1840
1860
1880
1900
1920
1940
1960
1980
2000
Time (yr)

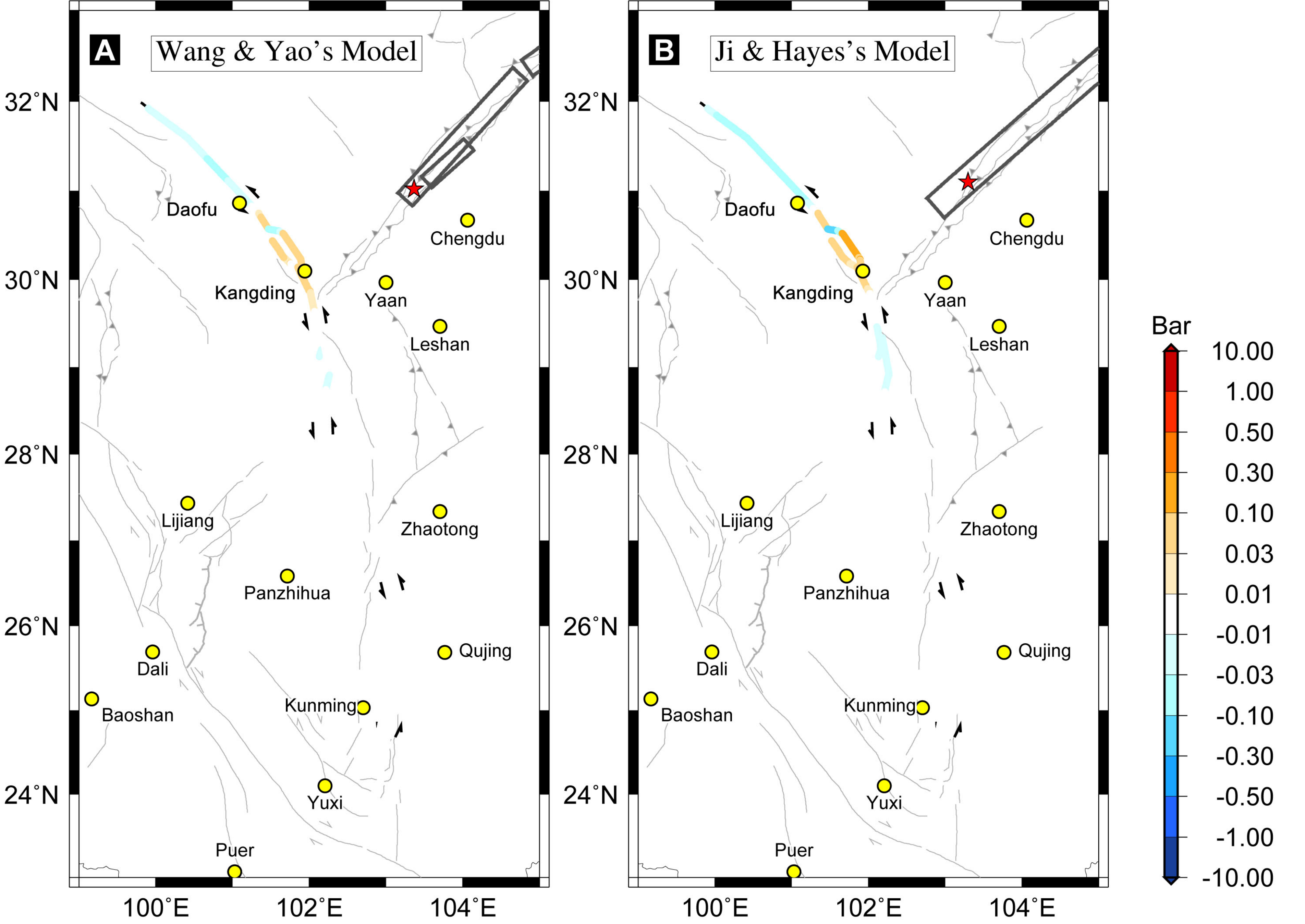

A
Wang & Yao's Model
B
Ji & Hayes's Model
32°N
30°N
28°N
26°N
24°N
100°E
102°E
104°E
Daofu
Kangding
Chengdu
Yaan
Leshan
Lijiang
Zhaotong
Panzhihua
Dali
Qujing
Baoshan
Kunming
Yuxi
Puer
Bar
10.00
1.00
0.50
0.30
0.10
0.03
0.01
-0.01
-0.03
-0.10
-0.30
-0.50
-1.00
-10.00